1 **Competition between myosin II and β_H-Spectrin regulates cytoskeletal tension**

2 Consuelo Ibar[1], Krishna Chinthalapudi[2], Sarah M. Heissler[2] and Kenneth D. Irvine[1]*

3 [1]Waksman Institute and Department of Molecular Biology and Biochemistry, Rutgers

4 University, Piscataway NJ 08854 USA

5 [2]Department of Physiology and Cell Biology, Dorothy M. Davis Heart and Lung Research

6 Institute, The Ohio State University College of Medicine, Columbus, Ohio, USA

7 *Corresponding author: irvine@waksman.rutgers.edu

8

9

ABSTRACT

Spectrins are membrane cytoskeletal proteins generally thought to function as heterotetramers comprising two α-spectrins and two β-spectrins. They influence cell shape and Hippo signaling, but the mechanism by which they influence Hippo signaling has remained unclear. We have investigated the role and regulation of the *Drosophila* β-heavy Spectrin (β_H-Spectrin, encoded by the *karst* gene) in wing imaginal discs. Our results establish that β_H-Spectrin regulates Hippo signaling through the Jub biomechanical pathway due to its influence on cytoskeletal tension. While we find that α-Spectrin also regulates Hippo signaling through Jub, unexpectedly, we find that β_H-Spectrin localizes and functions independently of α-Spectrin. Instead, β_H-Spectrin co-localizes with and reciprocally regulates and is regulated by myosin. In vivo and in vitro experiments support a model in which β_H-Spectrin and myosin directly compete for binding to apical F-actin. This competition can explain the influence of β_H-Spectrin on cytoskeletal tension and myosin accumulation. It also provides new insight into how β_H-Spectrin participates in ratcheting mechanisms associated with cell shape change.

24 **INTRODUCTION**

25 The spectrin cytoskeleton has been described as a lattice of cross-linked, spring-like
26 proteins that provide structural support to cells (Liem, 2016; Machnicka et al., 2014). Spectrins
27 were first discovered and characterized in red blood cells but are expressed in many cell types.
28 Spectrins can bind to cell membranes and F-actin, linking them together. They are generally
29 thought to act as heterotetramers, composed of two α subunits and two β subunits. *Drosophila* has
30 one α-spectrin (α-Spec) and two β-spectrins: β-Spectrin (β-Spec) and β-Heavy-Spectrin (β_H-Spec,
31 encoded by *karst* (*kst*)), which could potentially generate two distinct spectrin heterotetramers:
32 $(\alpha\beta)_2$ and $(\alpha\beta_H)_2$. β-Spec and β_H-Spec interact with F-actin through their N-terminal domains,
33 which contain two actin-binding calponin-homology (CH) domains, connecting the spectrin
34 cytoskeleton to the actin cytoskeleton (Liem, 2016). In *Drosophila* epithelia, it has been reported
35 that β-Spec localizes to the lateral sides of cells, β_H-Spec localizes to the apical sides of cells, and
36 α-Spec localizes both laterally and apically, leading to inferences that spectrin exists as lateral
37 $(\alpha\beta)_2$ tetramers and apical $(\alpha\beta_H)_2$ tetramers (Dubreuil et al., 1997; Lee et al., 1997; Thomas et al.,
38 1998; Zarnescu and Thomas, 1999). Despite common assumptions that spectrins act as tetramers,
39 there is some evidence that alternative arrangements may exist. In *Drosophila* ovarian follicle
40 cells, the absence of α-Spec diminishes the recruitment of β_H-Spec to the apical domain, but it does
41 not affect the recruitment of β-Spec to the lateral domain (Lee *et al.*, 1997). Examination in
42 *Drosophila* of a mutant form of α-Spec that, based on in vitro studies, is unable to bind β-spec and
43 compromised in its ability to bind β_H-Spec, revealed that it could nonetheless rescue the lethality
44 of an *α-Spec* mutant (Khanna et al., 2015). Experiments done with a mammalian homolog of β_H-
45 Spec, βV-Spec, showed that it can homodimerize through its C-terminal region, raising the
46 possibility that βV-Spec might be able to cross-link F-actin by itself (Papal et al., 2013).

47 Several studies have reported that spectrins also regulate Hippo signaling, with effects on
48 cell proliferation and readouts of Hippo signaling reported in *Drosophila* imaginal discs and
49 ovarian follicles, as well as in cultured mammalian cells (Deng et al., 2015; Deng et al., 2020;
50 Fletcher et al., 2015; Wong et al., 2015). Hippo signaling is a signal transduction network that
51 responds to diverse upstream inputs, including the cytoskeleton and cells' physical environment
52 (Misra and Irvine, 2018; Zheng and Pan, 2019). Hippo signaling largely modulates cell
53 proliferation and fate through the regulation of Yap family transcriptional co-activator proteins
54 (Yorkie, Yki, in *Drosophila*, YAP1 and TAZ in humans). Yki is primarily regulated through
55 phosphorylation by the kinase Warts (Wts), which promotes the cytoplasmic localization of Yki.
56 Various potential mechanisms for biomechanical regulation of Yki/Yap activity have been
57 described, but the best-characterized mechanism in *Drosophila* is the Jub biomechanical pathway.
58 This involves tension-dependent recruitment of an Ajuba LIM protein (Jub in *Drosophila*, LIMD1
59 in mammals) to α-catenin at adherens junctions (AJ) (Alegot et al., 2019; Ibar et al., 2018;
60 Rauskolb et al., 2022; Rauskolb et al., 2014; Sarpal et al., 2019; Sun et al., 2015). Jub then recruits
61 and inhibits Wts, resulting in increased Yki activity.

62 Studies of the influence of spectrins on Hippo signaling have suggested different
63 mechanisms by which this might occur (Deng *et al.*, 2015; Deng *et al.*, 2020; Fletcher *et al.*, 2015;
64 Wong *et al.*, 2015). Fletcher *et al.* (2015), focusing on β_H-Spec, suggested that the spectrin
65 cytoskeleton influences the membrane density, and thereby the activation state, of upstream
66 regulators of Hippo signaling. Wong *et al.* (2015), focusing on β-Spec, suggested that spectrins
67 might influence Hippo signaling by modulating levels of F-actin; increased levels of F-actin have
68 been reported in other studies to be associated with increased Yki/Yap activity (Aragona et al.,
69 2013; Fernandez et al., 2011; Sansores-Garcia et al., 2011). Deng *et al.* (2015), focusing on α-

70 Spec, reported that spectrins regulate levels of phosphorylated myosin light chain (required for
71 myosin activation) but surprisingly did not affect levels of myosin or recruitment of Jub, leading
72 them to infer that spectrins can act through a novel tension-dependent but Jub-independent
73 pathway. These same authors later reported that in the pupal eye, spectrins can act through Jub,
74 while suggesting that the action of spectrins in the pupal eye differs from their action in the wing
75 disc (Deng *et al.*, 2015; Deng *et al.*, 2020).

76 The disparate models for how spectrins influence Hippo signaling have led to confusion
77 over whether a distinct spectrin-based mechanism exists for the mechanical regulation of Hippo
78 signaling. We were particularly interested in investigating claims that spectrins could alter
79 cytoskeletal tension in wing discs without affecting Jub localization or levels of myosin. Our
80 results reveal that both β_H-Spec and α-Spec influence Jub recruitment to AJ, and their effects on
81 Yki activity depend upon Jub. Together, these observations argue that spectrins influence Hippo
82 signaling through the Jub biomechanical pathway. Unexpectedly, our investigations also reveal
83 that β_H-Spec and α-Spec act separately in wing discs - they do not co-localize, nor do they influence
84 each other's localization. These observations argue that β_H-Spec does not act as part of an $(\alpha\beta_H)_2$
85 tetramer in the wing disc but rather exerts its functions independently of α-Spec. Finally, we
86 establish that β_H-Spec and myosin reciprocally antagonize each other's apical localization in wing
87 discs - myosin inhibits β_H-Spec, and β_H-Spec inhibits myosin. We further show that β_H-Spec and
88 myosin can compete in vitro for binding to F-actin. Together with structural modeling, our
89 observations argue that β_H-Spec and myosin compete for binding to F-actin in vivo. This
90 competition could explain how β_H-Spec influences myosin activity and further suggests a simple
91 mechanism for the contribution of β_H-Spec to ratcheting processes that alter cell shape via
92 actomyosin contractility.

93

94 **RESULTS**

95 **β_H-spectrin regulates myosin activity and levels in wing imaginal discs**

96 Prior studies have reported that mutation or RNAi-mediated knockdown of spectrins in
97 wing and eye imaginal discs increased myosin activity, as visualized by staining for myosin light
98 chain phosphorylated at activation sites (pMLC) (Deng *et al.*, 2015; Forest et al., 2018).
99 Surprisingly, it was also reported that levels of myosin co-localizing with F-actin were nonetheless
100 unaffected (Deng *et al.*, 2015), whereas changes in myosin activity generally correlate with
101 changes in myosin accumulation (Fernandez-Gonzalez et al., 2009; Noll et al., 2017). To re-
102 examine this, we analyzed wing imaginal discs in which the apical, β_H-Spec *kst* was knocked down
103 in posterior cells by expressing UAS-RNAi lines under *en-Gal4* control. This increased apical
104 pMLC in posterior cells, where levels of β_H-Spec were reduced (Figure 1- figure supplement 1B
105 and D), consistent with previous reports (Deng *et al.*, 2015; Forest *et al.*, 2018). A difference in
106 junctional tension between anterior (control) cells and posterior (β_H-Spec RNAi) cells in our
107 experiments was confirmed by measuring the recoil velocity of cell junctions after laser cutting,
108 which demonstrated an increased tension in the β_H-Spec depleted sides (Figure 1I). To examine
109 myosin protein levels, we employed a widely-used myosin light chain GFP fusion, Sqh:GFP. We
110 found that depletion of β_H-Spec led to increased levels of junctional myosin (Figure 1B). To
111 quantify these effects on Sqh:GFP levels, we made maps of Sqh:GFP intensity normalized against
112 E-cad intensity. These are displayed on a red (high) to blue (low) heat map (Pan et al., 2018) and
113 calculated the ratio of intensities of the anterior (control) versus posterior (experimental)
114 compartments (Alegot *et al.*, 2019) (Figure 1E-H, J-K). This was further confirmed by using a

115 distinct β_H-Spec RNAi line (*UAS-kstRNAi*^{HMS00882}), which similarly increased myosin levels
116 (Figure 1- figure supplement 1E).

117 As earlier studies reporting no effect on myosin levels focused on mutation or knockdown
118 of α-Spec (Deng *et al.*, 2015), we considered the possibility that knockdown of α- and β_H-Spec
119 might differ in their effects on apical myosin accumulation. However, we found that knockdown
120 of α-Spec also caused an increased accumulation of apical myosin, as well as pMLC and junctional
121 tension, similar to the effects of β_H-Spec knockdown (Figure 1D, H, J, K; Figure 1- figure
122 supplement 1C and D). α-Spec and β_H-Spec knockdown differed though in that the thickness of
123 the wing disc epithelium was reduced by α-Spec knockdown, but not by β_H-Spec knockdown
124 (Figure 1- figure supplement 2).

125

126 **β_H-Spec regulates Hippo signaling through Jub**

127 It was previously argued that spectrins do not influence Hippo signaling through the Jub
128 biomechanical pathway in wing discs, in part based on an apparent lack of effect of *α-Spec*
129 mutation or depletion on Jub localization (Deng *et al.*, 2015). However, multiple studies have
130 consistently observed that Jub localization increases when tension at AJ is increased (Forest *et al.*,
131 2018; Pan *et al.*, 2018; Rauskolb et al., 2019; Rauskolb *et al.*, 2014; Razzell et al., 2018). Thus,
132 we examined Jub localization under conditions of β_H-Spec depletion. In wing imaginal discs, Jub
133 accumulates in puncta that often occur near intercellular vertices, together with a lower-level, more
134 even accumulation along the cell-cell junctions (Figure 2A and Figure 2– figure supplement 1C).
135 Jub is recruited by a tension-dependent conformational change of α-catenin, and Jub puncta are
136 increased when cytoskeletal tension is higher. Consistent with this, examination of Jub:GFP
137 confirmed that the increased junctional tension and myosin activity caused by β_H-Spec depletion

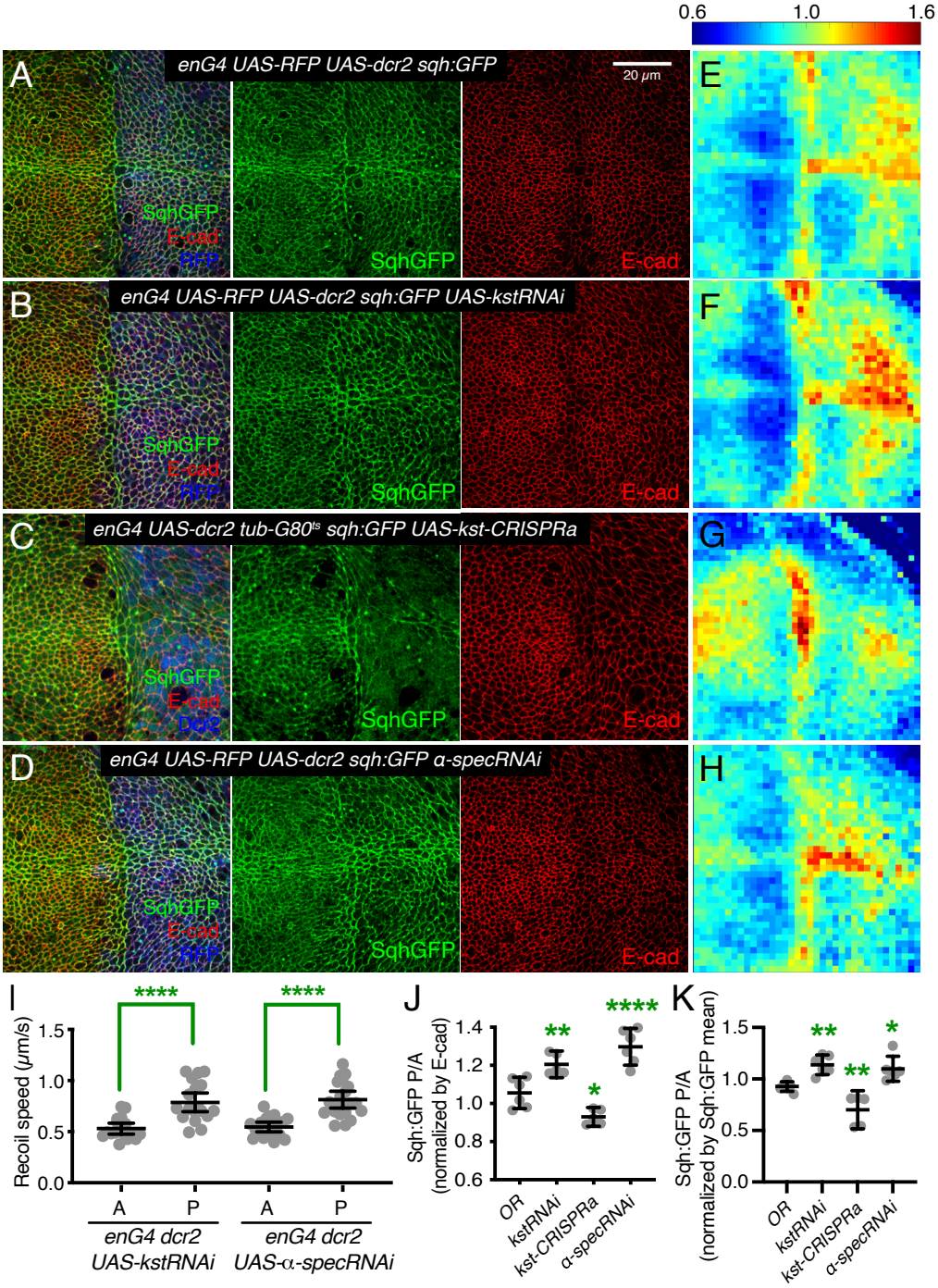

Figure 1. β_H-Spec and α-Spec reduce junctional myosin levels in wing discs
(A-D) Apical sections of wing imaginal discs expressing *en-Gal4 UAS-RFP UAS-dcr2 sqh:GFP* crossed to control (Oregon-R, OR) (A), *UAS-kstRNAi* (B), *UAS-kst-CRISPRa* (C), or *UAS-α-specRNAi* (D) showing the effect on Sqh:GFP (green) levels and localization in the posterior compartment (marked by RFP, blue). Scale bar = 20 µm; all images are at the same magnification. (E-H) Heat maps of relative junctional Sqh:GFP intensity of wing discs. Levels of Sqh:GFP relative to E-cad levels are shown for the different genotypes analyzed in A-D. Heat map scale is indicated on the top. Number of wing discs used for analysis: Control (OR), *n*=6; *UAS-kstRNAi*, *n*=5; UAS-kst-CRISPRa, *n*=5; *UAS-α-specRNAi*, *n*=6. (I) Average recoil velocities after laser cutting of cell junctions in anterior (A) or posterior (P) compartments of wing discs expressing *UAS-kstRNAi* or *UAS-a-specRNAi* in posterior cells (n=20). (J-K) Quantification of Sqh:GFP normalized to E-cadherin in posterior cells (P) compared to anterior cells (A) in wing disc expressing the indicated constructs, displayed as individual values, normalized by E-cad (J) or normalized by the mean intensity of Sqh:GFP (K). Data are shown as mean ± 95% CI. Statistical significance in (I) was determined by Student's t-test between A and P. For (J) and (K), statistical significance was determined by a one-way ANOVA with Dunnett's multiple comparison test relative to the control (Oregon-R): ns: not significant, *P<0.05; **P≤0.01; ***P≤0.001; ****P≤0.0001.

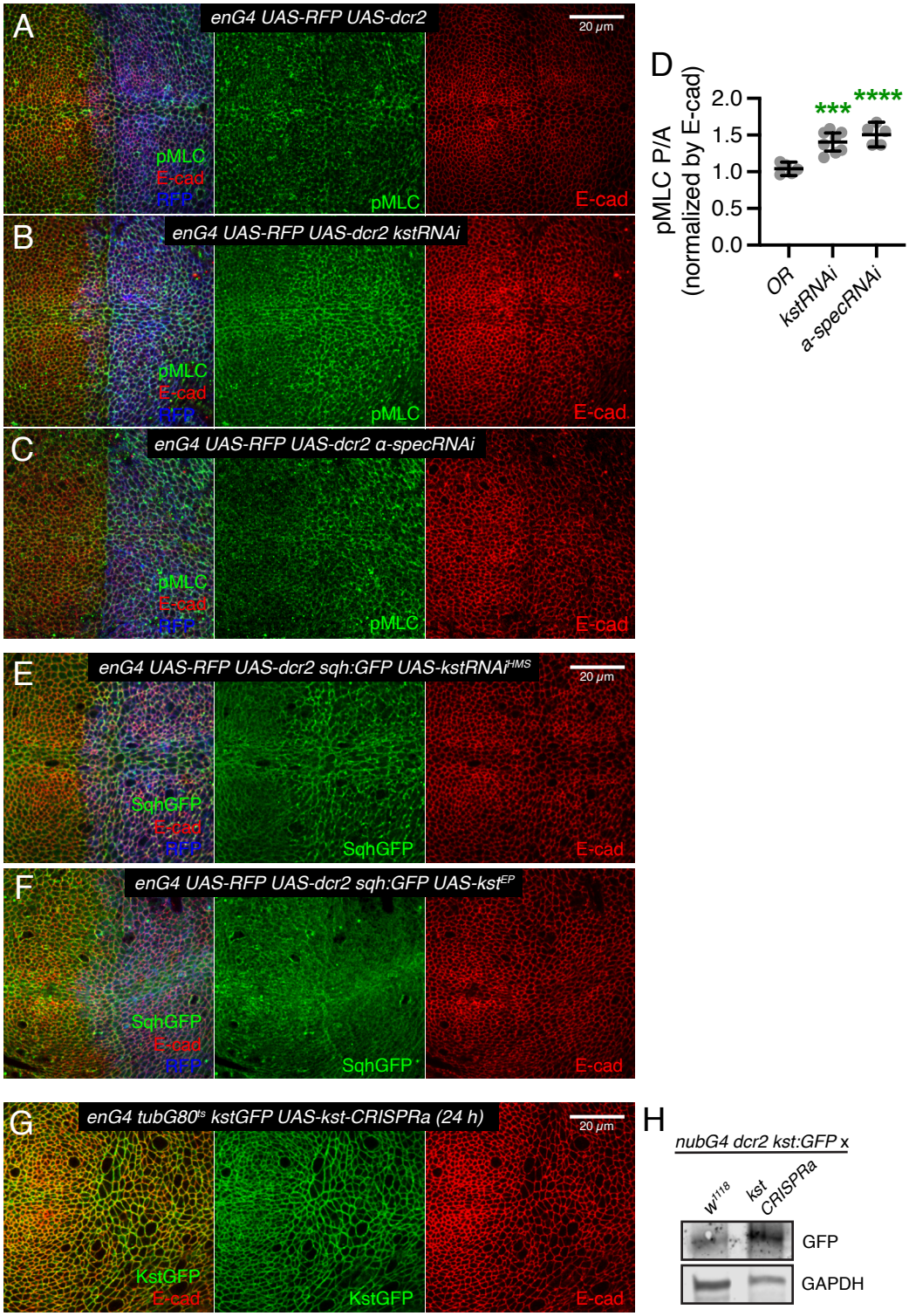

Figure 1 – figure supplement 1. Modulation of levels of total and active myosin in wing imaginal discs by β_H-Spec. (A-C) Apical sections of third instar wing imaginal discs expressing *en-Gal4 UAS-dcr2 UAS-RFP* (blue) crossed with control (A), *UAS-kstRNAi* (B) and *UAS-α-SpecRNAi* (C), stained with pMLC antibody (green) and E-cad (red). (D) Quantification of pMLC normalized to E-cadherin in posterior cells (P) compared to anterior cells (A) in wing discs expressing the indicated constructs, displayed as individual values. Number of wing discs used for analysis: Control (OR), n=5; *UAS-kstRNAi*, n=8, *UAS-α-SpecRNAi*, n=5. Error bars show mean with 95% CI. Statistical significance was determined by one-way ANOVA with Dunnett's multiple comparison test. Statistical comparisons are shown relative to the control (OR). ***P≤0.001, ****P<0.0001. (E-F) Third instar wing imaginal discs expressing en-Gal4 UAS-dcr2 UAS-RFP (blue) sqh:GFP (green) in combination with *UAS-kstRNAi*^{HMS00882} (E) and *UAS-kst*$^{P[EPgy2]EY01010}$ (F), stained for E-cad (red). (G) Apical sections of a wing imaginal disc expressing *en-Gal4 tubG80*^{ts} *kst:GFP* crossed with *UAS-kstCRISPRa*, stained for E-cad (red). Expression of Kst:GFP (green) was induced by transferring the flies from 18ºC to 29ºC for 24 h. (H) Western blots of wing disc lysates with the genotypes shown in the figure: *nub-Gal4 UAS-Dcr2 kst:GFP* crossed with w1118 (control) and *UAS-kstCRISPRa* (experimental). Kst:GFP was detected using a GFP antibody. GAPDH was used as a loading control.

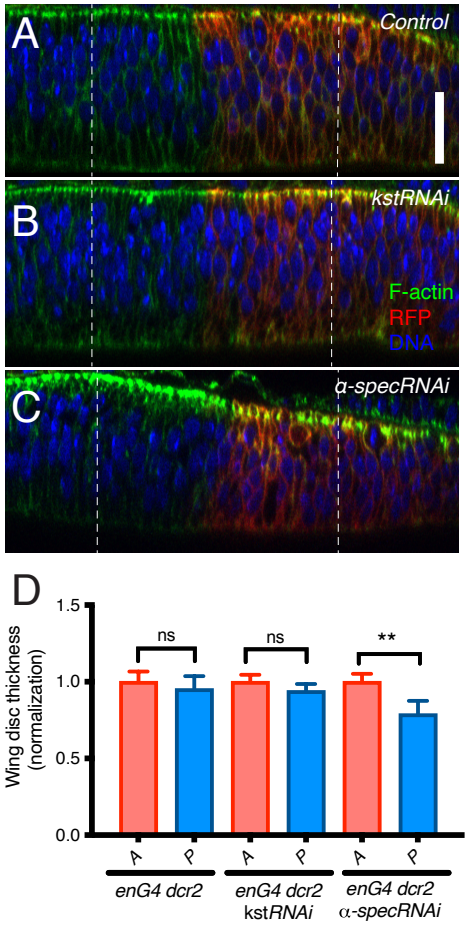

Figure 1 – figure supplement 2. α-Spec knockdown affects wing imaginal disc thickness.
(A-C) Lateral views of wing imaginal discs expressing *en-Gal4 UAS-RFP UAS-dcr2* crossed with control (Oregon-R, OR) (A), *UAS-kstRNAi* (B) or *UAS-α-specRNAi* (C), immunostained with phalloidin to label F-actin (green), Hoechst to label nuclei (blue) and the posterior compartment marked by RFP (red). Dashed lines indicate 30 µm from the center. Scale bar = 20 µm (D) Quantification of wing imaginal disc thickness determined 30 µm from the center in anterior (A) and posterior (P) sides for the different genotypes indicated. Statistical significance was determined by Student's t-test. ns: not significative; **P≤0.01; ***P≤0.001

138 is associated with increased junctional recruitment of Jub (Figure 2B, F, I-J and Figure 2 -figure
139 supplement 1D).

140 To assess the functional significance of increased Jub localization to AJ under β_H-Spec
141 knockdown conditions, we assayed the ability of RNAi-mediated *jub* knockdown to suppress β_H-
142 Spec RNAi phenotypes. Knockdown of β_H-spec throughout the developing wing under *nub-Gal4*
143 control increases wing size (wings were 116% and 119% of *nub-Gal4 UAS-dcr2* control size for
144 the two different UAS-RNAi lines used) (Figure 3A, C-D and K) (Deng *et al.*, 2015; Fletcher *et*
145 *al.*, 2015). Knockdown of *jub* leads to smaller wings (Das Thakur et al., 2010; Rauskolb et al.,
146 2011). In animals with simultaneous RNAi knockdown of *jub* and *kst,* wing size is similar to that
147 of *jub* RNAi wings (Figure 3B, E-F and K). The epistasis of *jub* to *kst* suggests that β_H-Spec
148 regulates wing size through its tension-dependent regulation of Jub.

149 To confirm that the relationship between Jub and β_H-Spec revealed by analysis of adult
150 wing size corresponds to changes in Hippo pathway activity, we analyzed the expression of a
151 transcriptional reporter of *ex*, *ex-lacZ*, which is a direct target of Yki (Hamaratoglu et al., 2006).
152 Knockdown of β_H-Spec in posterior compartments through the expression of UAS-*kst* RNAi under
153 *en-Gal4* control caused a mild increase in *ex-lacZ* expression compared to the anterior
154 compartment and to control posterior compartments (Figure 3M). Knockdown of *jub* reduces *ex-*
155 *lacZ* expression (Das Thakur *et al.*, 2010; Rauskolb *et al.*, 2011). Simultaneous RNAi knockdown
156 of *jub* and *kst* reduced *ex-lacZ* expression, similar to that in *jub* RNAi cells (Figure 3N-O). The
157 suppression of the influence of *kst* on Hippo signaling is again consistent with the inference that
158 β_H-Spec regulates Hippo signaling through the Jub biomechanical pathway.

159 As claims that spectrins act independently of Jub in wing discs were based primarily on
160 analysis of α-Spec, we also examined the effect of α-Spec knockdown on Jub levels. When α-Spec

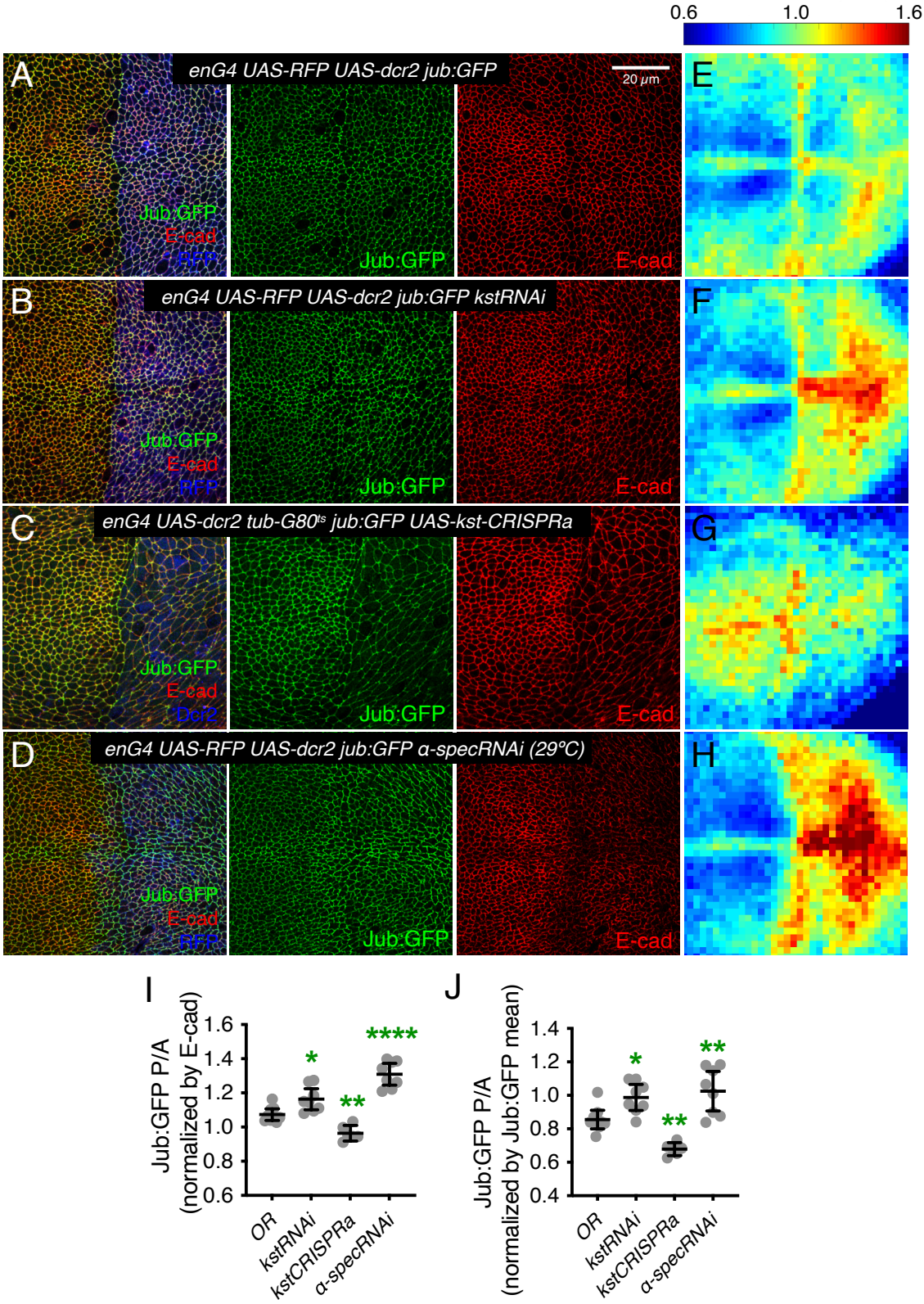

Figure 2. β_H-Spec and α-Spec reduce junctional Jub levels in wing discs

(A-D) Apical sections of wing imaginal discs expressing *en-Gal4 UAS-RFP UAS-dcr2 jub:GFP* crossed to control (Oregon-R, OR) (A), and *UAS-kstRNAi* (B), *UAS-kst-CRISPRa* (C) and *UAS-α-specRNAi* (D) showing the effect on Jub:GFP (green) levels and localization in the posterior compartment (marked by RFP, blue). Scale bar = 20 µm. (E-H) Heat maps of relative junctional Jub:GFP intensity of wing discs. Levels of Jub:GFP relative to E-cad levels are shown for the different genotypes analyzed. Heat map scale is indicated on the top. Number of wing discs used for analysis: Control (OR), *n*=9; *UAS-kstRNAi*, *n*=8; *UAS-kst-CRISPRa*, *n*=6; *UAS-α-specRNAi*, *n*=8. (I-J) Quantification of Jub:GFP normalized to E-cadherin (I) or to Jub:GFP mean intensity (J) in posterior cells compared to anterior cells (P/A) in wing discs expressing the indicated constructs, displayed as individual values. Data are shown as mean ± 95% CI, error bars show 95% CI. Statistical significance was determined by one-way ANOVA with Dunnett's multiple comparison test relative to the control (Oregon-R): ns: not significant, *P<0.05; **P≤0.01; ***P≤0.001; ****P≤0.0001

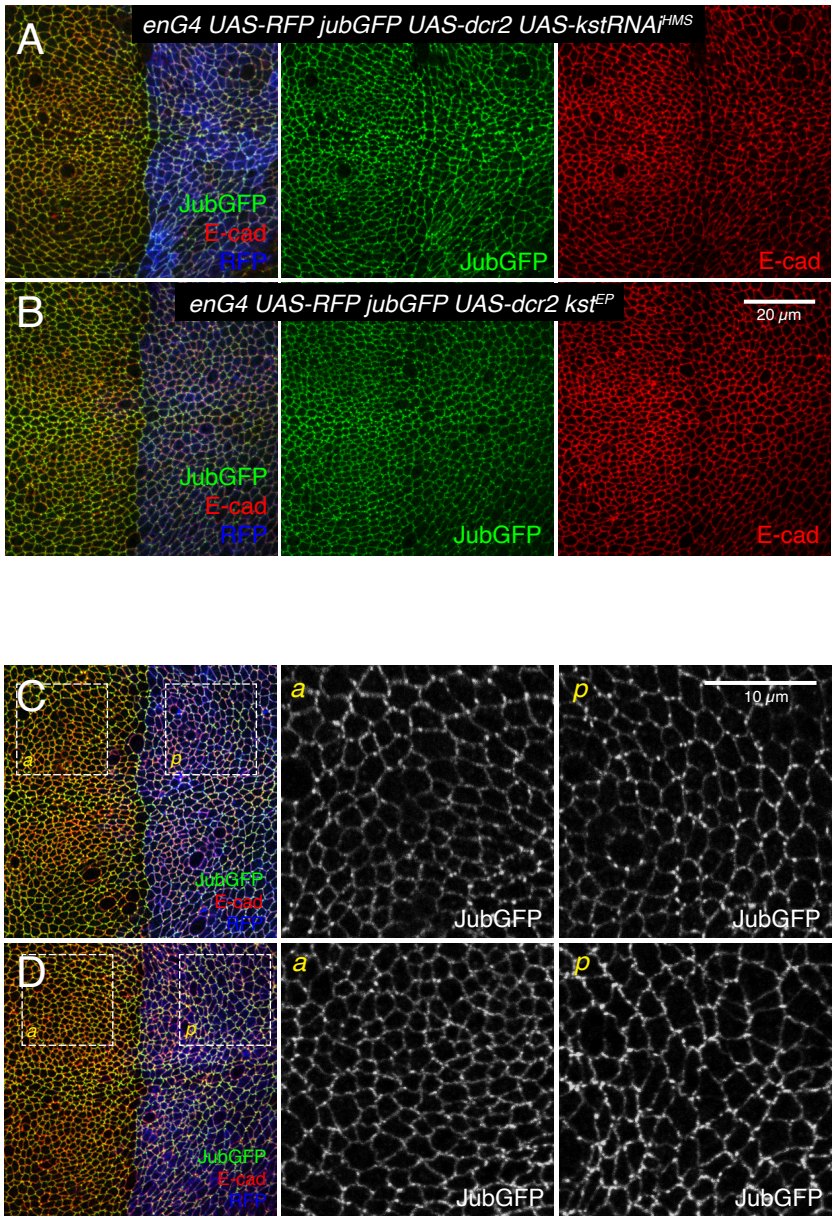

Figure 2 – figure supplement 1. β_H-spec modulates the recruitment of Jub:GFP to AJs.
(A, B) Third instar wing imaginal discs expressing *en-Gal4 UAS-dcr2 UAS-RFP* (blue) *jub:GFP* (green) in combination with *UAS-kstRNAi*^{HMS00882} (A) or *UAS-kst*$^{P[EPgy2]EY01010}$ (B) stained for E-cad (red). (C, D) Apical sections of wing imaginal discs expressing *en-Gal4 UAS-RFP UAS-dcr2 jubGFP* crossed to control (Oregon-R, OR) (C), *UAS-kstRNAi* (D) from Figure 2. Columns to the right show higher magnification views of the anterior (a) and posterior boxes (p).

161 was knocked down in posterior cells by *en-Gal4* driven RNAi, we observed that recruitment of
162 Jub to cell junctions was increased (Figure 2D, H-J). Moreover, as for β_H-Spec, we found that the
163 increased wing size and *ex-lacZ* expression caused by knockdown of α-Spec were suppressed by
164 knockdown of *jub* (Figure 3G, H, K and P-Q). Thus, as for β_H-Spec, and as suggested for pupal
165 eyes (Deng *et al.*, 2020), our observations imply that α-Spec also regulates Hippo signaling
166 through Jub in wing discs.
167

168 **β_H-Spec localizes independently from α-Spec in wing disc cells**

169 Prior studies of spectrin function in imaginal discs have assumed that they function as
170 heterotetramers, with an apical complex composed of $(\alpha\beta_H)_2$ subunits and a lateral complex
171 composed of $(\alpha\beta)_2$ subunits (Deng *et al.*, 2015; Deng *et al.*, 2020; Fletcher *et al.*, 2015; Thomas *et*
172 *al.*, 1998), as was originally suggested for ovarian follicle cells (Lee *et al.*, 1997). However, our
173 examination of spectrin localization in wing imaginal discs suggested that the apical-most
174 distributions of α-Spec and β_H-Spec differ. To directly compare them, we used an antibody against
175 α-Spec (Dubreuil et al., 1987) and a fully functional genomic YFP-trap of β_H-Spec (Kst:YFP) (Lye
176 et al., 2014). β_H-Spec is localized, as reported previously, at the apicobasal level of the adherens
177 junction in wing discs (Fletcher *et al.*, 2015; Forest *et al.*, 2018) (Figure 4A and C). Conversely,
178 α-Spec is enriched in a sub-apical region just below this, with slightly lower levels extending all
179 along the lateral membrane (Figure 4B and C). Only very low levels of α-Spec are detected in the
180 apical plane where β_H-Spec is detected, and their distributions in this plane appear to differ (Figure
181 4A and Figure 4 – figure supplement 1A).

182 To confirm that β_H-Spec and α-Spec localize independently of each other in wing discs,
183 we examined the consequences of depleting α-Spec, β-Spec, or β_H-Spec on each other's

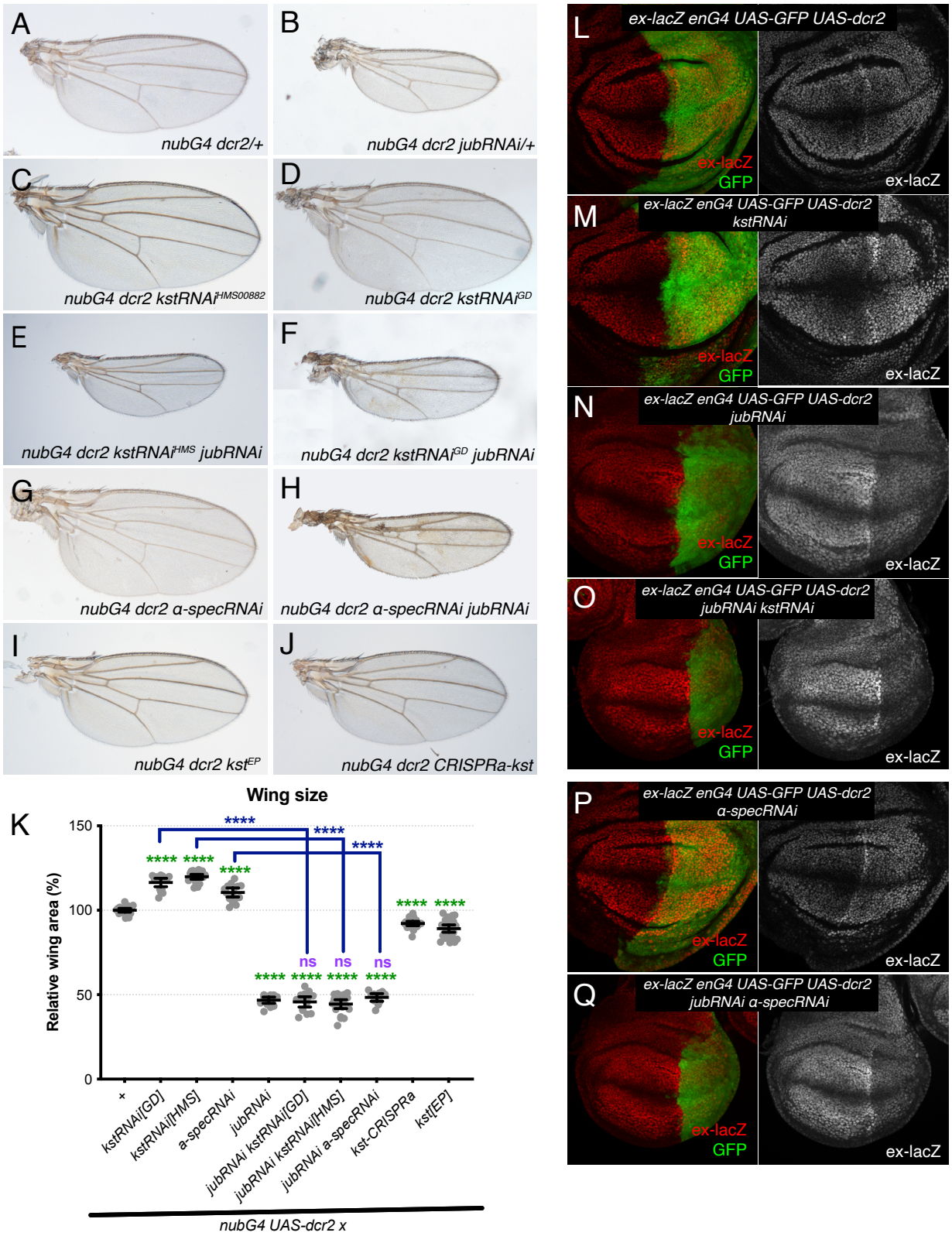

Figure 3. Jub is required for β_H-Spectrin and α-Spec regulation of wing size and ex-lacZ
(A-J) Adult wings from flies cultured at 29ºC and expressing UAS transgenes altering spectrin and/or jub expression under control of a *nub-Gal4* driver. Representative adult wings are shown. (K) Quantification of wing area (mean ± 95% CI, n > 20). Statistical significance was determined by a one-way ANOVA with Tukey's multiple comparison test. Statistical comparisons are shown relative to *nub-Gal4 UAS-dcr2/+* in green or relative to *nub-Gal4 UAS-dcr2 UAS-jubRNAi/+* in purple. Additional selected statistical comparisons are shown in blue. (L-Q) Third-instar wing imaginal discs expressing *ex-lacZ en-Gal4 UAS-dcr2 UAS-GFP* (green) crossed to OR (L), *UAS-kstRNAi* (M), *UAS-jubRNAi* (N), *UAS-jubRNAi UAS-kstRNAi* (O), *UAS-α-specRNAi* (P), *UAS-jubRNAi UAS-α-specRNAi* (Q) stained for expression of ex-lacZ (red/white).

184 localization. For this, we used *en-Gal4* driven UAS-RNAi lines to knockdown one of the spectrin
185 proteins, and then examined whether the localization of the others was affected. These experiments
186 revealed, as expected, that β-Spec knockdown does not significantly affect β_H-Spec localization
187 (Figure 4E), but it does strongly reduce α-Spec localization (Figure 4 – figure supplement 1C). α-
188 Spec knockdown does not affect β_H-Spec apical localization (Figure 4D) but slightly reduces β-
189 Spec localization (Figure 4 – figure supplement 1B). Finally, β_H-Spec depletion does not affect α-
190 Spec localization (Figure 4F). These observations suggest that while α-Spec needs β-Spec to
191 localize to lateral membranes, the localization of β_H-Spec and α-Spec are functionally independent.
192 Together with the distinct localization of these proteins revealed by imaging, these observations
193 argue against the existence of $(\alpha\beta_H)_2$ complexes in wing imaginal discs.
194

195 **β_H-Spec and apical myosin antagonize each others' localization to apical F-actin**

196 The discovery that β_H-Spec and α-Spec localize independently led us to consider what
197 factors might influence the apical localization of β_H-Spec. Intriguingly, the distribution of β_H-Spec
198 in wing disc cells appears very similar to the apical distribution of F-actin and myosin, and
199 similarities between the localization of β_H-Spec and myosin in *Drosophila* embryos have been
200 noted previously (Krueger et al., 2020; Thomas and Kiehart, 1994). To determine whether myosin
201 and β_H-Spec colocalize in wing discs, we imaged discs expressing GFP-tagged β_H-Spec (Kst:GFP)
202 and mCherry-tagged myosin light chain (Sqh:mCherry). This revealed extensive co-localization
203 between these proteins in the apical region of wing disc epithelial cells (Figure 5A and B).
204 Quantitation of these images yielded a Pearson's Correlation Coefficient score of 0.636 (for
205 comparison, the Pearson's Correlation Coefficient score between Kst:YFP and α-Spec is 0.18
206 (Figure 4A)).

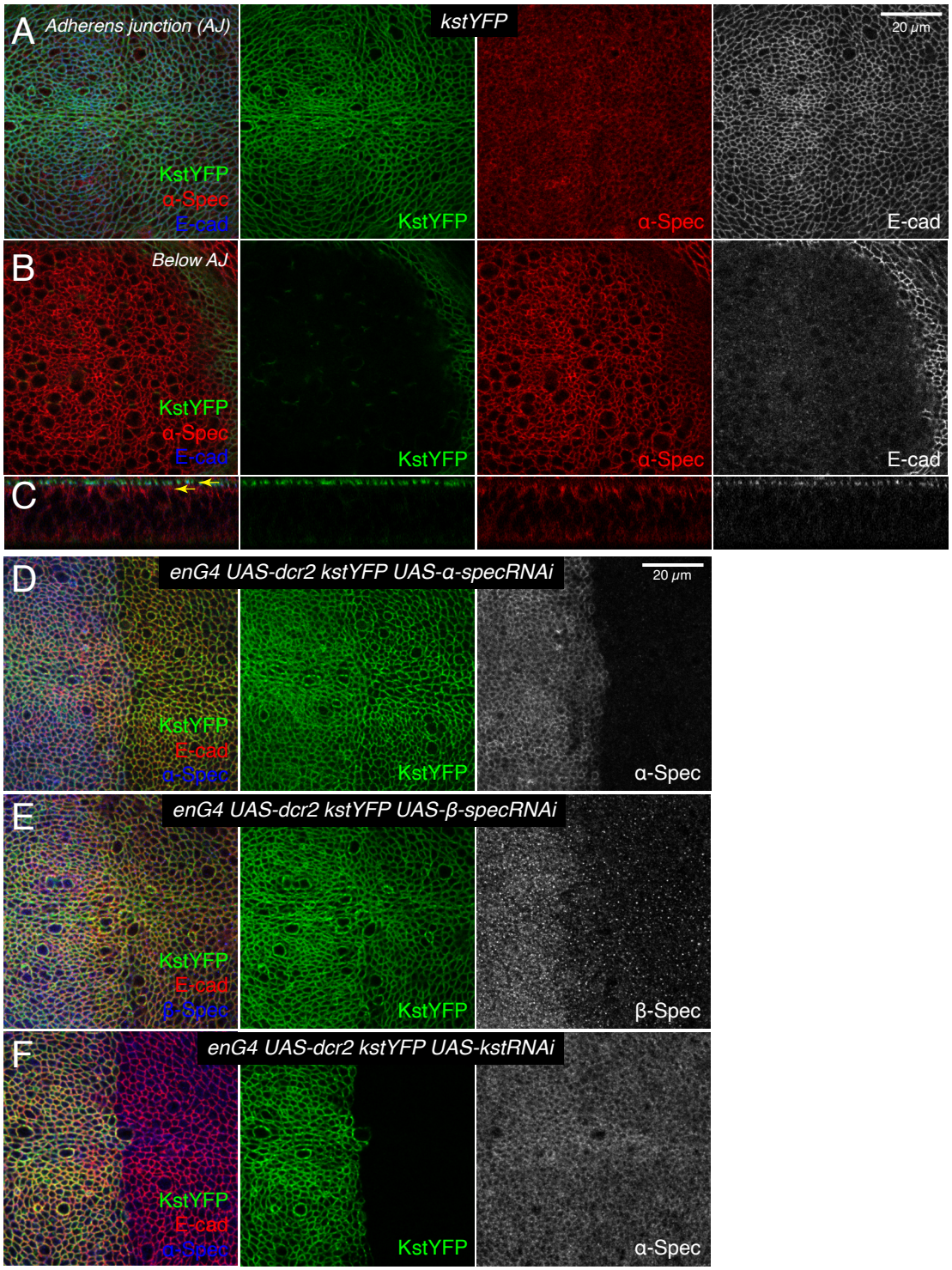

Figure 4. β_H-Spec and α-Spec localize independently in wing imaginal discs.
(A-C) Wing imaginal discs expressing Kst:YFP immunostained with α-Spec and E-cad antibodies showing the localization of β_H-Spec (Kst:YFP) and α-Spec at the AJ (A), below the AJ (B) and in cross sections (C). Upper yellow arrow in cross section indicates AJ layer, lower yellow arrow indicates "Below AJ" layer. (D-F) Apical sections of wing imaginal discs expressing *en-Gal4 UAS-dcr2 kstYFP* along with *UAS-α-specRNAi* (D), *UAS-β-specRNAi* (E) and *UAS-kstRNAi* (F) immunostained with α-Spec (D and F) or β-Spec antibodies (E), validating the different RNAi lines used and showing that the apical localization of βH-Spec (Kst) is independent of the presence of α-Spec or β-Spec. Scale bar = 20 µm. The AJ layers were obtained by ImSAnE, using as a reference the E-cad channel and 7 layers were projected (2.1 µm).

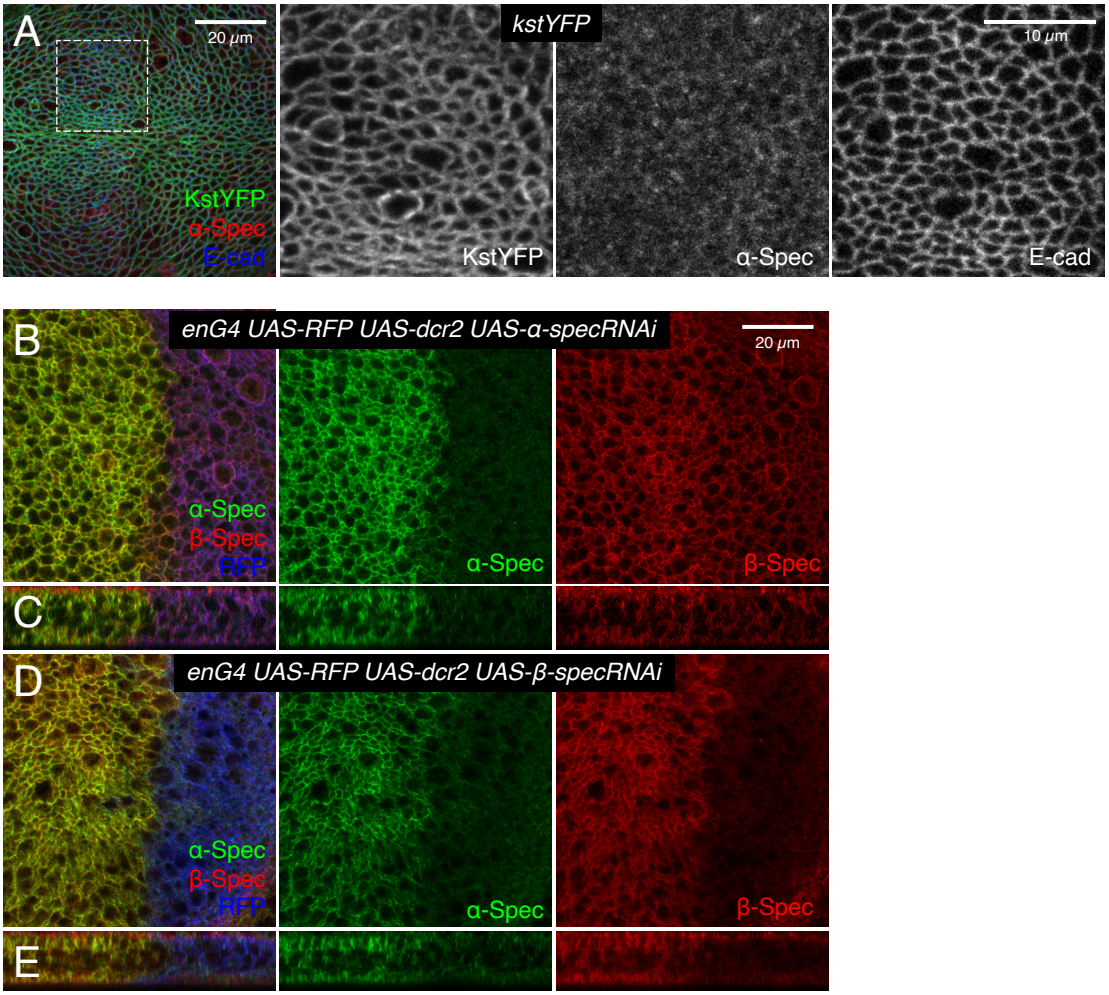

Figure 4 – figure supplement 1. Loss of β-Spec affects α-Spec localization in wing discs.
(A) Higher magnification of the different channels in the boxed region indicated in A (from Figure 4A). (B-E) Sections of a wing imaginal disc expressing *en-Gal4 UAS-RFP UAS-dcr2* crossed with *UAS-α-specRNAi* (B-C) or *UAS-β-specRNAi* (D-E) with lateral views (C, E) stained with mouse α-Spec (green) and rabbit β-Spec (red) antibody. Scale bar = 20 μm.

207 The extensive co-localization of β_H-Spec and myosin prompted us to investigate the
208 functional relationship between them further. As noted above, reduction of β_H-Spec leads to
209 increased apical myosin levels and activity. To investigate whether myosin reciprocally regulates
210 β_H-Spec, we expressed transgenes that modulate actomyosin contractility. RNAi-mediated
211 knockdown of Rho kinase (Rok) reduces myosin activity by reducing phosphorylation of myosin
212 light chain (MLC, encoded in *Drosophila* by *spaghetti squash* (*sqh*)). In wing discs, knockdown
213 of *Rok* is also associated with reduced recruitment of myosin to apical junctions (Rauskolb *et al.*,
214 2014), consistent with the generally positive correlation between myosin activity and co-
215 localization with F-actin (Fernandez-Gonzalez *et al.*, 2009; Noll *et al.*, 2017). Conversely,
216 examination of β_H-Spec in wing disc cells expressing *Rok* RNAi revealed increased levels of β_H-
217 Spec along apical junctions (Figure 5D). To increase myosin activity, we expressed a constitutively
218 activated, phosphomimetic form of myosin light chain, Sqh^{EE} (Winter et al., 2001). This increases
219 the recruitment of myosin to AJ (Rauskolb *et al.*, 2014), but decreases the recruitment of β_H-Spec
220 to AJ, and a portion of β_H-Spec instead appears in apical vesicles (Figure 5E). To quantify these
221 effects on β_H-Spec levels, we made maps of β_H-Spec intensity normalized against E-cad intensity,
222 displayed on a red (high) to blue (low) heat map (Pan *et al.*, 2018). Calculation of the ratio of
223 intensities of the anterior (control) versus posterior (experimental) compartments further
224 confirmed our observation that myosin antagonizes localization of β_H-Spec to AJ (Figure 5G-J).
225 Thus, β_H-Spec and myosin II localization to AJ are affected in opposite ways by changes in
226 cytoskeletal tension.

227 The opposing effects of changes in myosin activity on myosin and β_H-Spec localization,
228 together with the observation that loss of β_H-Spec leads to increased myosin activity and apical
229 localization, raised the possibility that myosin and β_H-Spec compete for localization to apical F-

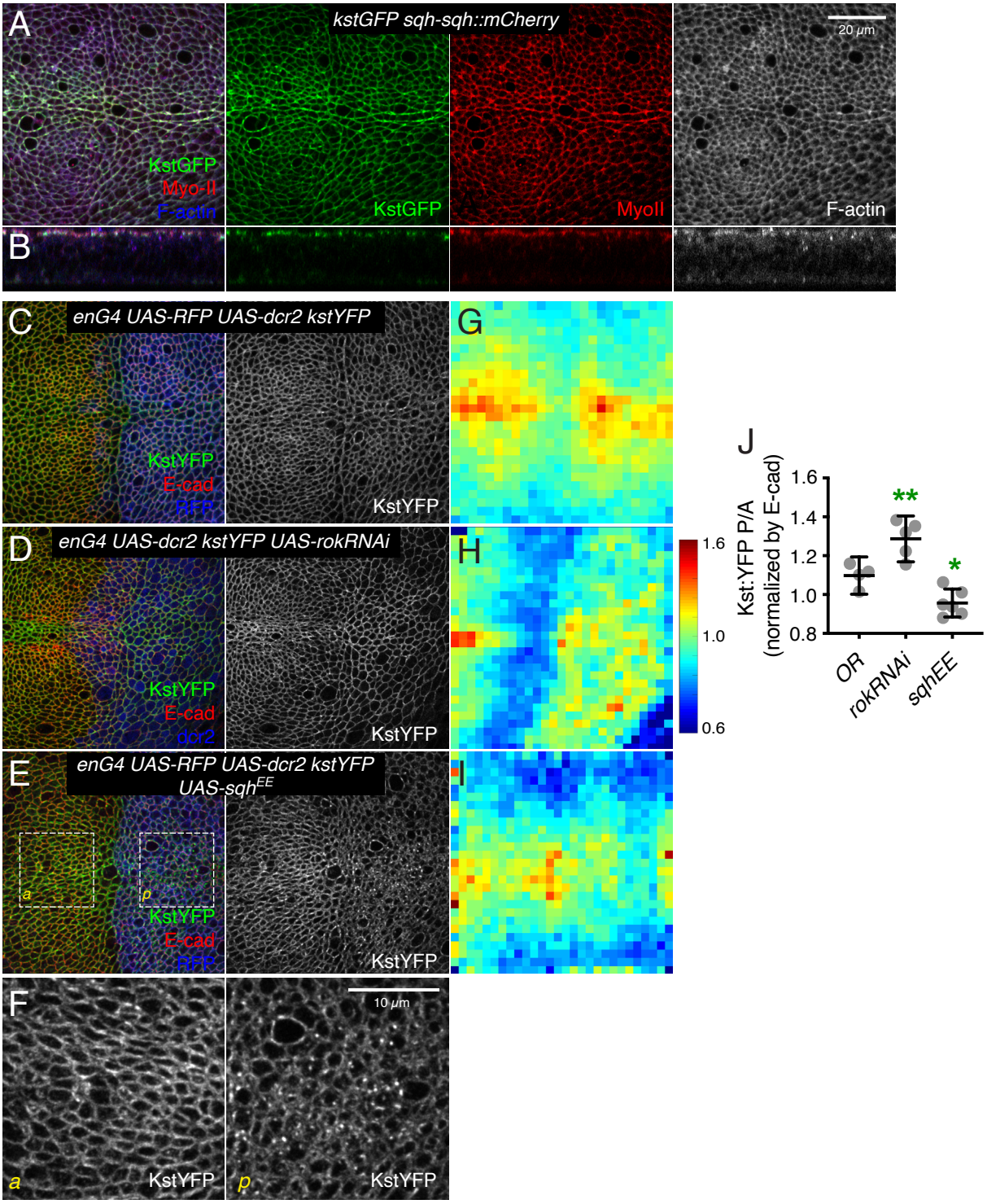

Figure 5. β_H-Spec colocalizes with myosin and is regulated by myosin activity

(A-B) Wing imaginal disc co-expressing Kst:GFP and the myosin II reporter sqh-sqh::mCherry in apical views (A) and lateral views (B), co-stained with phalloidin for F-actin (blue/white). (C-E) Apical sections of wing discs expressing *en-Gal4 UAS-RFP UAS-dcr2 kst:YFP* crossed to (Oregon R, OR) (C), *UAS-rokRNAi* (D) or *UAS-sqh^{EE}* (E) in the posterior compartment (marked by RFP, blue), showing the effect of altering myosin activity on the Kst:YFP localization (gray). Scale bar = 20 µm. (F) Higher magnification of the boxed regions indicated in E. Scale bar = 10 µm (G-I) Heat maps of junctional Kst:GFP intensity relative to E-cad of wing discs (n=5, for each genotype) are shown. Heat map scale is on the right side. (J) Quantification of Kst:YFP intensity normalized to E-cadherin in posterior cells (P) compared to anterior cells (A) in wing discs expressing the indicated constructs (n=5). Data are shown as mean ± 95% CI, error bars indicate CI. Statistical significance was determined by a one-way ANOVA with Dunnett's multiple comparison test relative to the control (Oregon-R): ns: not significant, *P<0.05; **P≤0.01.

230 actin. To further investigate this possibility, we overexpressed β_H-Spec using a CRISPR-activator
231 (CRISPRa) approach. This involves the expression of a transcriptional activator fused to dCas9
232 under UAS control, which can then be recruited to a gene of interest using a single-guide RNA
233 (sgRNA) targeted upstream of the transcription start site (Jia et al., 2019; Jia et al., 2018). To verify
234 the overexpression of β_H-Spec, we employed it in flies with GFP-tagged β_H-Spec at the
235 endogenous locus (Kst:GFP). To avoid excessive cell death caused by Kst overexpression we
236 expressed this construct under inducible conditions, using the temperature-sensitive Gal4 repressor
237 $Gal80^{ts}$. Both imaging and western blotting of wing discs confirmed that this CRISPRa approach
238 effectively increased expression of Kst:GFP (Figure 1 - figure supplemental 1G-H). Examination
239 of myosin under β_H-Spec overexpression conditions, using Sqh:GFP, revealed a substantial
240 reduction of myosin localization to AJs (Figure 1C, G, J-K). Apical cell areas were also increased,
241 consistent with a reduction of junctional tension (Figure 1C). As an independent method to
242 overexpress β_H-Spec, we used a previously described EP-element insertion near *kst*,
243 P[EPgy2]EY01010 (UAS-kst^{EP}) (Pogodalla et al., 2021). Over-expression of β_H-Spec using UAS-
244 kst^{EP} under *en-Gal4* control also reduced myosin levels at AJ (Figure 1 – figure supplemental 1F),
245 although the effect appeared weaker than that induced by the CRISPRa approach. These results
246 provide further evidence that β_H-Spec antagonizes myosin recruitment to AJs and establish that
247 this effect can be observed under both increased and decreased β_H-Spec expression conditions.
248 Consistent with these reductions in apical myosin accumulation, β_H-Spec overexpression
249 also reduced junctional recruitment of Jub (Figure 2C, G, I-J and Figure 2 – figure supplement
250 1B) and decreased wing size (wings were 92% and 89% of *nub-Gal4 UAS-dcr2* control size, for
251 the two different overexpression constructs) (Figure 3I-K).
252

253 **β_H-Spec and myosin compete for binding to F-actin**

254 The reciprocal antagonism between myosin and β_H-Spec suggested that they could compete
255 for binding to F-actin. β_H-Spec contains two N-terminal actin-binding domains, CH1 and CH2
256 (Liem, 2016), and myosin contains an actin-binding region in its motor domain (Duan et al., 2018).
257 While spectrins and myosin have been purified and characterized in vitro, we lack a mechanistic
258 understanding of the interaction between β_H-Spec and F-actin and how it might affect myosin
259 binding. To address this, we conducted in vitro co-sedimentation assays with purified protein
260 domains and F-actin. We found that the isolated *Drosophila* β_H-Spec actin-binding region binds
261 F-actin weakly (Figure 6A), in agreement with previous reports of F-actin binding by other spectrin
262 CH1-CH2 domains (Avery et al., 2017; Duan *et al.*, 2018). Constitutively active *Drosophila*
263 Myosin II (subfragment-1-like protein) binding to F-actin appears stronger than β_H-Spec binding,
264 as at the same concentration a greater fraction of Myosin II is bound to F-actin (Figure 6B). To
265 investigate the antagonism between these proteins observed in vivo, we performed biochemical
266 competition assays between the β_H-Spec CH domains and myosin for binding to F-actin. F-actin
267 was preincubated with an excess of β_H-Spec CH domains to saturate binding sites on F-actin, and
268 then increasing concentrations of myosin were added. We found that myosin can displace the actin-
269 binding region of β_H-Spec from F-actin by ~50% at the highest myosin concentration that we could
270 use (Figure 6C, bottom). Myosin binding to F-actin was unaffected by preincubation with β_H-Spec
271 CH domains (Figure 6 – figure supplement 1A), likely due to myosin's higher binding affinity for
272 F-actin.

273 To gain a structural understanding of the antagonism between β_H-Spec and myosin we built
274 homology models of the *Drosophila* CH1-CH2 domain of β_H-Spec and the myosin II motor
275 domain and compared them with previous cryo-EM structures of the human actin-bound β-III-

276 spectrin actin binding CH1 domain and actin-bound myosin (Avery *et al.*, 2017; von der Ecken et
277 al., 2016). The superimposition of the isolated *Drosophila* β_H-Spec CH1 domain model on the
278 human β-III spectrin CH1 domain in a complex with F-actin structure revealed a binding site
279 between actin subdomains (SD) SD1 and SD2 along the filament (Figure 6D). The binding region
280 of myosin on F-actin includes SD1, SD2, and SD3 (Figure 6D). The superimposition of both
281 models suggests that the binding position of the CH1 domain on F-actin sterically interferes with
282 the formation of a strong actin-myosin interface (Figure 6D''). Modeling of the β_H-Spec CH1-
283 CH2 domain indicates that the CH2 domain presents additional steric hindrance for myosin
284 binding to F-actin (Figure 6 – figure supplement 1B-B''). Thus, structural modeling suggests that
285 the binding of spectrin or myosin to individual binding sites on F-actin is mutually exclusive,
286 which could explain why they compete with each other for F-actin association in vivo and in vitro.
287

288 **DISCUSSION**

289 Multiple models for how spectrins regulate Hippo signaling have been proposed (Deng *et*
290 *al.*, 2015; Deng *et al.*, 2020; Fletcher *et al.*, 2015; Wong *et al.*, 2015). We focused on investigating
291 claims that spectrins could alter cytoskeletal tension in wing discs by regulating pMLC levels
292 without affecting localization of myosin or Jub (Deng *et al.*, 2015). In contrast to prior studies, we
293 observed that when β_H-Spec or α-Spec levels are decreased by RNAi, levels of junctional myosin
294 are increased. This increase in junctional myosin levels is associated with increased junctional
295 tension and with increased recruitment of Jub to AJ. We are not certain why these effects were
296 missed in prior studies, but we note that our observations are consistent with studies linking
297 recruitment of both myosin and Jub to AJ under tension (Alegot *et al.*, 2019; Fernandez-Gonzalez
298 *et al.*, 2009; Ibar *et al.*, 2018; Noll *et al.*, 2017; Rauskolb *et al.*, 2019; Rauskolb *et al.*, 2014; Razzell

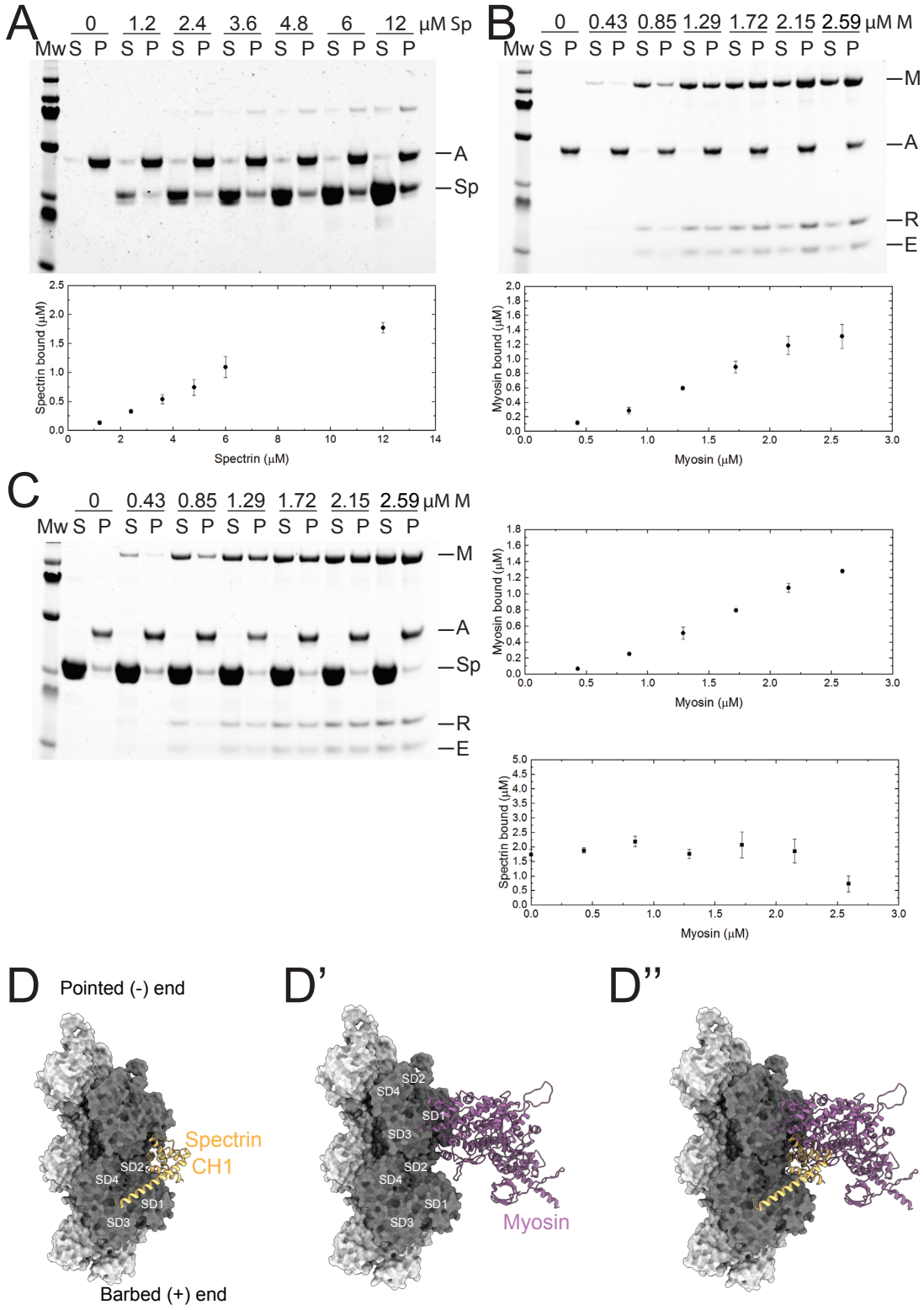

Figure 6. Spectrin and myosin have overlapping binding sites on F-actin.
(A-C) Co-sedimentation assays with β_H-Spec CH domains (Spectrin), F-actin, and myosin-II subfragment-1-like protein (myosin). For all sedimentation assays, A, M, Sp, E, and R refer to F-actin, myosin heavy chain, spectrin, myosin essential light chain and myosin regulatory light chain, respectively. Mw indicates marker and S and P refer to supernatant and pellet, respectively. Quantification shows mean ± S.D. of the sedimentation behavior of spectrin and myosin with F-actin (n = 3). (A) Co-sedimentation assay between spectrin (0-12 μM) and F-actin (2 μM). (B) Co-sedimentation assay between myosin (0-2.59 μM) and F-actin (2 μM). (C) Co-sedimentation assay between spectrin (12 μM), myosin (0-2.59 μM) and F-actin (2 μM). Quantification shows that myosin reduces spectrin binding by ~50% (bottom panel). (D-D'') Model of the Drosophila CH1 domain (yellow) bound to F-actin (grey) (D). Model of the Drosophila myosin motor domain (purple) bound to F-actin (grey) (D'). Superimposition of the CH1 and myosin motor domain on F-actin. The two strands of the actin filament are shown in light and dark grey and subdomains are indicated.

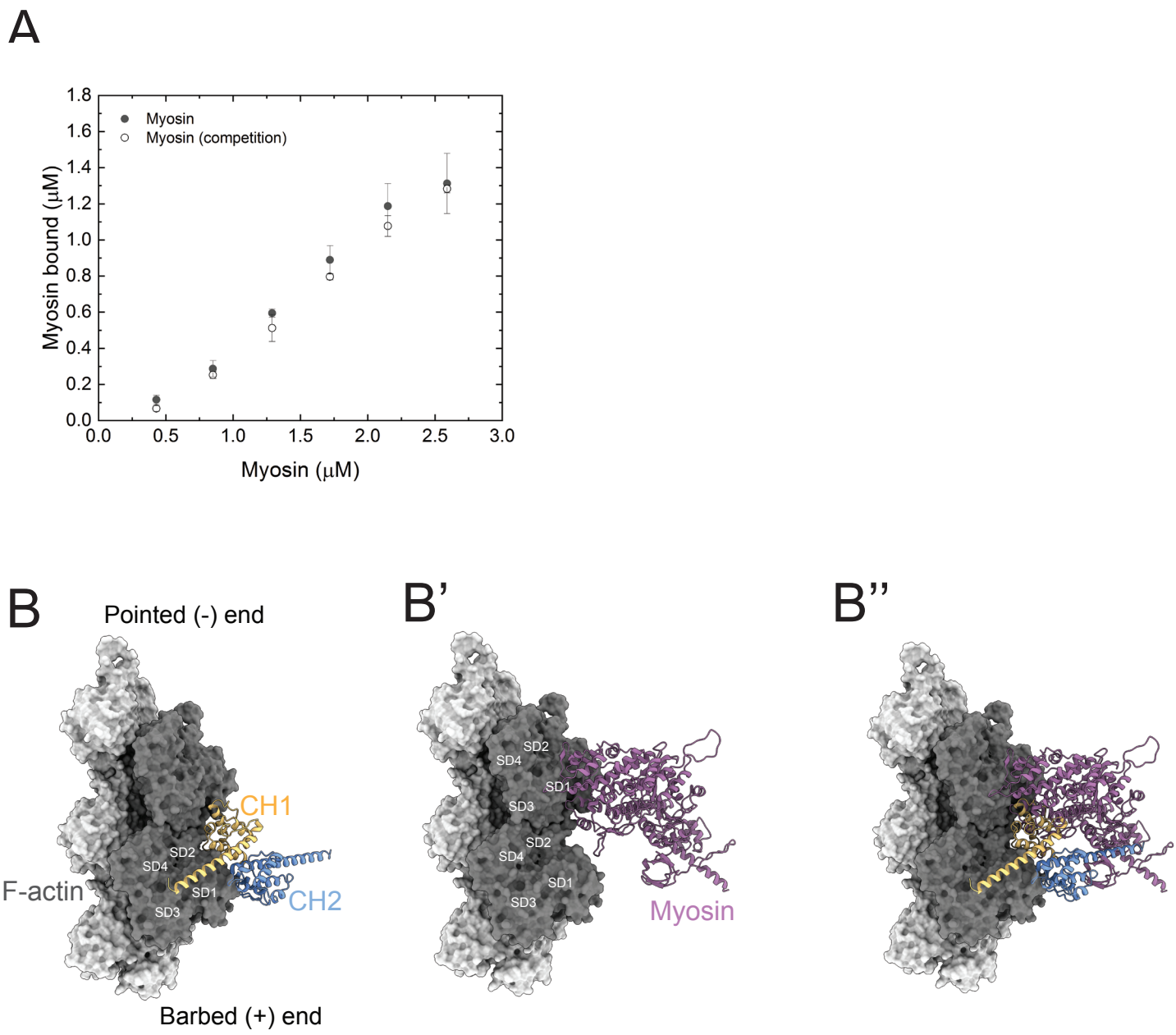

Figure 6 – figure supplement 1. Additional examination of competition between spectrin and myosin for F-actin.

(A) Quantification of the binding behavior of myosin to F-actin in the presence and absence of spectrin in co-sedimentation assays. The similarity in actin binding indicates that pre-loading spectrin does not interfere with myosin binding to F-actin under these assay conditions. (B) Model of the Drosophila CH1-CH2 domain (CH1, yellow; CH2, blue) bound to F-actin (grey) (B'). Model of the Drosophila myosin motor domain (purple) bound to F-actin (grey) (B''). Superimposition of the CH1-CH2 and myosin motor domain on F-actin. The two strands of the actin filament are shown in light and dark grey and subdomains are indicated.

299 *et al.*, 2018; Sarpal *et al.*, 2019). Moreover, our results are further supported by the observation
300 that *jub* is genetically required for the influence of spectrin knockdown on Yki activity and wing
301 growth. Taken together, these observations indicate that β_H-Spec and α-Spec regulate Hippo
302 signaling in wing discs through the Jub-biomechanical pathway, rather than through hypothesized
303 alternate mechanisms.

304 Spectrin has been suggested to form two distinct complexes in *Drosophila* epithelial cells,
305 $(\alpha\beta)_2$ and $(\alpha\beta_H)_2$ heterotetramers, which localize to the lateral and apical sides of cells, respectively
306 (Deng *et al.*, 2015; Dubreuil *et al.*, 1997; Fletcher *et al.*, 2015; Lee *et al.*, 1997; Thomas *et al.*,
307 1998; Zarnescu and Thomas, 1999). However, our observations indicate that β_H-Spec functions
308 independently of α-Spec in wing imaginal discs. α-Spec and β_H-Spec do not exhibit significant co-
309 localization. Moreover, α-Spec and β_H-Spec are not required for each other's localization to apical
310 cell junctions. This contrasts with the requirement for β-Spec for recruitment of α-Spec to lateral
311 membranes in wing discs. The requirement is not entirely reciprocal, as α-Spec knockdown only
312 partially reduces β-Spec recruitment, but this likely reflects mechanisms that recruit spectrins to
313 cell membranes: β-spectrin subunits, but not α-spectrin subunits, have a pleckstrin homology
314 domain that can mediate membrane association, as well as possessing the CH domains that mediate
315 F-actin association. Without these, and without β-Spec, α-Spec does not have a way to associate
316 with lateral membranes.

317 An independent role for β_H-Spec has also been suggested in mammalian photoreceptors,
318 where it was reported that that mammalian βV-Spec does not colocalize with αII-spectrin, and that
319 βV-spec could form homodimers, potentially allowing it to cross-link actin by itself, enabling α-
320 Spec-independent functions (Papal *et al.*, 2013). The observation that a mutation in *Drosophila* α-
321 Spec that disrupts binding to β-Spec *in vitro* has only mild phenotypes also suggests that spectrin

322 functions do not depend entirely on αβ interactions (Khanna *et al.*, 2015). Collectively, our results
323 together with these earlier studies emphasize that the dogma that "Spectrin comprises α-and β-
324 subunits that interact in an antiparallel manner to form an αβ dimer" (Liem, 2016) should be
325 revised.

326 The conclusion that β_H-Spec and α-Spec act independently implies that they influence
327 tension at apical junctions through distinct mechanisms. α-Spec might influence AJ tension in
328 wing discs through the mechanism proposed to explain the influence of α- and β-Spec in pupal
329 eyes (Deng *et al.*, 2020). It was inferred that α- and β-Spec maintain cell rigidity by linking F-actin
330 to membranes. In the absence of α- or β-Spec, it was proposed that dissociation between F-actin
331 and the membrane leads to an expansion of the cell cortex. This cell shape change increases
332 cytoskeletal tension at AJs, which bind F-actin independently of spectrins. Consistent with this,
333 we observed a decrease in cell height in α-Spec knockdown cells in wing discs. These alterations
334 in cell shape were not observed in β_H-Spec knockdown cells, further supporting the conclusion
335 that β_H-Spec and α-Spec act independently to regulate junctional tension.

336 Instead, our experiments analyzing the relationship between β_H-Spec and myosin revealed
337 an entirely different mechanism by which β_H-Spec influences tension at AJ. We observed a mutual
338 antagonism between β_H-Spec and myosin *in vivo* for localization to apical F-actin: decreasing β_H-
339 Spec increases junctional myosin, while increasing β_H-Spec decreases junctional myosin.
340 Reciprocally, increasing myosin activity decreases β_H-Spec localization to apical F-actin, while
341 decreasing myosin activity increases β_H-Spec localization to apical F-actin. In vitro studies with
342 purified protein domains revealed that myosin can compete with β_H-Spec for binding to F-actin.
343 Finally, computational modeling of protein structures revealed that myosin and β_H-Spec would
344 interfere with each other's binding to F-actin. Together, these observations indicate that β_H-Spec

345 and myosin directly compete with each other for localization to F-actin. The influence of β_H-Spec
346 on junctional tension is thus a direct consequence of its competition with myosin for overlapping
347 binding sites on F-actin.

348 Despite β_H-Spec and myosin sharing overlapping binding sites on F-actin, and competing
349 reciprocally in vivo, in our co-sedimentation experiments we could only detect a partial ability of
350 myosin to compete for β_H-Spec binding, and we could not detect an ability of β_H-Spec to compete
351 for myosin binding. Several factors are likely to contribute to these observations. First, we could
352 not use higher protein concentrations of myosin or β_H-Spec due to the need to keep the salt
353 concentration constant and close to physiological levels, and to prevent protein precipitation.
354 Second, it has been suggested for β-Spec that the CH2 domain regulates the actin binding function
355 of the CH1 domain through steric hindrance when the two domains are associated (Avery *et al.*,
356 2017). A specific mutation in β-Spec CH2 (L253P) has been shown to lower the energetic barrier
357 between closed and open structural states, increasing the affinity of β-Spec for F-actin around
358 1000-fold (Avery et al., 2016), but it is unknown how β-Spec or β_H-Spec conformational changes
359 are normally regulated in vivo and whether both proteins share this regulatory feature.
360 Additionally, phosphorylation of myosin regulatory light chain shifts myosin from a compact,
361 autoinhibited conformation to a filamentous, active conformation (Kiehart and Feghali, 1986;
362 Vasquez et al., 2016). The autoinhibited conformation binds F-actin very weakly (K_D>100 μM)
363 (Heissler and Manstein, 2013; Sellers et al., 1982) compared to the active conformation, suggesting
364 that spectrin could outcompete autoinhibited myosin more effectively than active myosin for
365 binding to F-actin. In addition, other factors including other actin-binding proteins and cytoskeletal
366 tension are likely to influence the dynamic localization and actin-binding properties of both
367 proteins (Duan *et al.*, 2018; Greenberg et al., 2016).

368 The competition between β_H-Spec and myosin also provides key insights into how β_H-Spec
369 contributes to ratcheting of apical constriction. The apical constriction of cells in the ventral furrow
370 that initiates *Drosophila* mesoderm invagination occurs through fast constriction pulses
371 interrupted by pauses during which cells must stabilize their constricted state before reinitiating
372 constriction (Martin et al., 2009; Xie and Martin, 2015). This ratcheting-like behavior is thought
373 to be a consequence of the finite length of actin filaments. Myosin contracts the cytoskeleton by
374 driving filaments past each other, and extensive contractions require release and reassociation with
375 new pairs of filaments. β_H-Spec participates in ratcheting of apical constriction (Krueger et al.,
376 2020). When β_H-Spec is knocked down, cells can undergo cycles of unratcheted apical constriction
377 during which they alternately constrict and then expand. Consequently, most β_H-Spec depleted
378 embryos fail to complete normal mesoderm invagination. It was proposed that the actin cross-
379 linking function of β_H-Spec could hold F-actin in place for the next cycle of myosin mediated-
380 contraction, but this raises the question of how myosin and β_H-Spec association with F-actin are
381 coordinated so that β_H-Spec prevents relaxation without interfering with constriction. Our results
382 suggest a simple solution: since they compete for the same binding site, the release of myosin from
383 F-actin at the end of a cycle of contraction would naturally be coupled to the accessibility of F-
384 actin for binding by β_H-Spec. Thus the competition between myosin and β_H-Spec for binding to F-
385 actin enables myosin-mediated cell contraction to effectively alternate with β_H-Spec-mediated
386 stabilization.
387
388 **MATERIALS AND METHODS**
389 ***Drosophila* genetics**

390 Unless otherwise indicated, crosses were performed at 29°C. Protein localization and
391 expression levels were monitored using previously characterized transgenes: *ex-lacZ*
392 (Hamaratoglu *et al.*, 2006), *kst:YFP* (Lye *et al.*, 2014), *kst:GFP* (Nagarkar-Jaiswal et al., 2015),
393 *jub:GFP* (Sabino et al., 2011), *sqh:GFP* (Royou et al., 2004) and *sqh:mCherry* (Martin *et al.*,
394 2009).

395 To manipulate gene expression in the posterior compartment, *en-Gal4 UAS-RFP; UAS-*
396 *dcr2* flies were crossed with to UAS-RNAi or overexpression lines. RNAi transgenes used were
397 *UAS-kstRNAi* (v37075), *UAS-kstRNAi* (HMS00882), *UAS-α-specRNAi* (v25387), *UAS-β-*
398 *specRNAi* (GL01174), *UAS-rokRNAi* (v104675) and *UAS-jubRNAi* (v38442). To increase myosin
399 activity, we used *UAS-sqh*^{EE} (Winter *et al.*, 2001) and to increase β_H-Spec levels, we used *UAS-*
400 *kstCRISPRa* (this paper) and *UAS-kst*$^{P[EPgy2]EY01010}$ (Pogodalla *et al.*, 2021).

401

402 **DNA Cloning**

403 To overexpress β_H-Spec, we used a second-generation CRISPR/Cas9-transcriptional
404 activation approach (Jia et al., 2018), allowing us to recruit the transcriptional machinery near the
405 transcription start site (TSS) of *kst* under UAS control. For this, we made the following primers to
406 generate a gRNA located less than 400 nt from the TSS: 5'-
407 TTCGGATAAGCCGACAGGGTCTAT and 5'-AAACATAGACCCTGTCGGCTTATC-3'
408 These primers were duplexed and cloned in the FlySAM 2.0 vector using the BbsI site (Jia et al.,
409 2019). Transgenic flies were made by injection (BestGene).

410 The actin binding domain (aa 1-278) of *kst* was cloned into pGEX-3X at the EcoRI site,
411 using the following primers: 5'-gatctgatcgaaggtcgtggaATGACCCAGCGGGACGGC-3' and 5'-
412 atcgtcagtcagtcacgatgTTACTTCTTGCGATCTGCGTCCATTAGC-3', and assembled using

413 NEBuilder® HiFi DNA Assembly (New England Biolabs, E2621) to generate plasmid pGEX-3X-
414 ABDkst.
415
416 **Histology and Imaging**
417 For most experiments wing discs were fixed in 4% paraformaldehyde for 15 min at room
418 temperature. Sqh:GFP discs were fixed for 12 min. Primary antibodies used were mouse anti-α-
419 Spectrin (1:50, Developmental Studies Hybridoma Bank, 3A9, RRID:AB_528473), rabbit anti-β-
420 spectrin (1:100, a gift from Christian Klämbt) (Hulsmeier et al., 2007), rabbit anti-Dcr2 (1:800,
421 Abcam, ab4732, RRID:AB_449344), rabbit anti-pMLC (T18/S19) (1:50, Cell Signaling
422 Technologies, #3671, RRID:AB_330248), rat anti-E-cad (1:200, Developmental Studies
423 Hybridoma Bank, DCAD2-c, RRID:AB_528120), mouse β-galactosidase (1:200, Developmental
424 Studies Hybridoma Bank, JIE7, RRID:AB_528101). Secondary antibodies were used at a 1:100
425 dilution, and included anti-rat Alexa Fluor 647 (Jackson ImmunoResearch, 712-605-153,
426 RRID:AB_2340694), anti-rabbit Alexa Flour 647 (Jackson ImmunoResearch, 711-605-152,
427 RRID:AB_2492288), anti-mouse Alexa Fluor 647 (Jackson ImmunoResearch, 715-605-151,
428 RRID:AB_2340863), anti-mouse Cy3 (Jackson ImmunoResearch, 715-165-151,
429 RRID:AB_2315777), anti-rabbit Cy3 (Jackson ImmunoResearch, 711-165-152,
430 RRID:AB_2307443), anti-rat Cy3 (Jackson ImmunoResearch, 712-165-153,
431 RRID:AB_2340667), anti-mouse Alexa Fluor 488 (Thermo Fisher Scientific, A-21202,
432 RRID:AB_141607) and anti-rabbit Alexa Flour 488 (Thermo Fisher Scientific, A-21206,
433 RRID:AB_2535792). DNA was stained using Hoechst (Invitrogen, H3570). Wing discs were
434 removed and mounted on a slide in Vectashield (Vector Laboratories, H-1000). Confocal images
435 were captured on a Leica SP8 microscope.

436

437 **Immunobloting**

438 Wing discs (20 discs per lane) were lysed in 2× Laemmli Sample Buffer (Bio-Rad,
439 #1610737) supplemented with protease inhibitor cocktail (Roche) and phosphatase inhibitor
440 cocktail (Calbiochem). Protein samples were loaded in 4% to 15% gradient gels (Bio-Rad).
441 Antibodies used for immunoblotting include mouse anti-GFP (1:1000; Cell Signaling Technology,
442 #2955, RRID:AB_1196614) and as a loading control rabbit anti-GAPDH (1:5000; Santa Cruz
443 Biotechnology, sc-25778, RRID:AB_10167668). Blots were visualized with fluorescent-
444 conjugated secondary antibodies (LI-COR Biosciences) and the Odyssey Imaging System (LICOR
445 Biosciences).

446

447 **Laser ablation**

448 Live imaging and laser ablation experiments were performed as previously described
449 (Rauskolb *et al.*, 2014). *en-Gal4 UAS-RFP/CyO; UAS-dcr2/TM6B* flies were crossed with *UAS-*
450 *kstRNAi; Ubi-E-cad:GFP/TM6B* flies. Eggs were collected at 25ºC for 4 hours and then shifted to
451 29°C for 88 h. Wing disc culture was based on the procedure of (Dye et al., 2017). A stock medium
452 was prepared using Grace's medium (Sigma, G9771) without sodium bicarbonate but with the
453 addition of 5 mM Bis-Tris and the pH was adjusted to 6.6-6.7 at room temperature. This was stored
454 at 4°C for less than a month. Before every experiment, we added 5% fetal bovine serum (FBS;
455 ThermoFisher, 10082147), Penicillin-Streptomycin (Thermo-Fisher, #15070063, 100X stock
456 solution) and 10 nM 20-hydroxy-ecdysone (Sigma, H5142) to the medium. Larvae were floated
457 on 25% sucrose and transferred into glass dishes with culture medium. Larvae of the desired
458 genotype were selected and sterilized in 70% ethanol for 1 min. Then, we drew a circle on the

459 glass bottom of a 35-mm glass-bottomed Petri dish (MatTek, P35G-0-14-C) using glue made by
460 mixing heptane with tape (Tesa, 5388). Wing discs were dissected out of larvae, transferred into
461 this Petri dish, and oriented using tungsten needles. Then we covered the discs with a Cyclopore
462 Polycarbonate membrane (GE Health, 7060-2513) and glued it to the glass bottom to immobilize
463 discs. Discs were imaged every 0.2 s on a Perkin Elmer Ultraview spinning disc confocal
464 microscope, and ablation of junctions was achieved using a Micropoint pulsed laser (Andor
465 Technology) tuned to 365 nm. Paired cutting of junctions, one in the anterior compartment and
466 another in the posterior compartment at a similar location, were performed and compared. The
467 displacement of vertices for the first second after ablation was used to calculate the velocities.

468 **Quantification and Statistical Analysis**

469 To obtain the surface of the wing disc and remove signals from the peripodial epithelium,
470 we used the MATLAB toolbox ImSAnE (Heemskerk and Streichan, 2015) to detect and isolate a
471 slice of the disc epithelium that surrounds the adherens junctions, using E-cad as a reference, as
472 described previously (Pan et al., 2016). The KstGFP, KstYFP, SqhGFP and JubGFP images were
473 created using ImSAnE. For septate junctions images, the surface detector was moved just below
474 the E-cadherin level.

475 For the fluorescence intensity heat maps, a custom MATLAB script was used (Alegot *et*
476 *al.*, 2019; Pan *et al.*, 2018) (https://github.com/alegoth/Wing-disc-Intensity-Analysis). The script
477 generates a 3D mask with the normalization channel (E-cad) keeping only the relevant pixels. The
478 wing disc center (intersection between AP/DV boundaries) is picked for each image manually.
479 Then, the picture is split into blocks of a given *xy* size (3×3 μm), starting from the center, and the
480 average intensity per pixel of each channel is measured. The intensity of the reference channel and
481 the channel of interest are normalized over their respective average intensity. The ratio of the

482 channel of interest over the reference channel is then determined. To average several discs, only
483 matrices of the same *xy* size blocks were used. The center of the disc serves as a reference point;
484 smaller matrices were expanded to correspond to the size of the biggest matrix and filled with NaN
485 (Not-a-Number). We determined the minimum number of values required (usually three) to
486 average the ratio for a given position. This means that the edges of the average disk are composed
487 of the same minimum number of values, which corresponds to the *n* given for each experiment.
488 Finally, signals from several wing discs were averaged and represented by the heat map, and a
489 posterior versus anterior ratio was calculated.

490 Pearson's correlation coefficient was calculated to establish co-localization between
491 different proteins by using the Coloc 2 Plugin for ImageJ (https://imagej.net/plugins/coloc-2).

492 Statistical significance was determined with GraphPad Prism software by performing
493 Student's t-test (for comparison between two observations) or analysis of variance (ANOVA) with
494 $P<0.05$ set as the criteria for significance. The Dunnett test was used to derive adjusted P-values
495 for comparisons against the control experimental value, and the Tukey test was used to derive
496 adjusted P-values for multiple comparisons.

497

498 **Protein production and purification**

499 To purify the actin binding domain of β_H-Spec fused with GST, we transformed BL21-
500 DE3 cells (NEB) with pGEX-3X-ABDkst. Protein expression was induced with 0.2 mM
501 isopropyl-β-D-thiogalactoside (IPTG) at room temperature for 12–15 h. Cells were harvested and
502 lysed by sonication in lysis buffer: PBS (pH 7.4), 1% Triton X-100, 5 mM dithiothreitol, 1 mM
503 phenylmethyl sulfonyl fluoride and complete Mini Protease Inhibitor Cocktail (Roche). After
504 centrifugation, the supernatant was collected and passed through a 1 mL GST-Trap column

505 (Cytiva) at 4 °C. Then, the column was washed with PBS (pH 7.4) until the absorbance reached a
506 steady baseline. To remove the GST-tag, the column was loaded with 80 units of Factor Xa (New
507 England Biolabs, P8010) in cleavage buffer: 50 mM Tris-HCl, 150 mM NaCl, 1 mM $CaCl_2$, pH
508 7.5 and incubated for 16 h at room temperature. To elute the ABD of β_H-Spec while removing the
509 protease simultaneously, we used a HiTrap Benzamidine FF (Cytiva) column in tandem with the
510 GST-trap column and eluted the ABD of β_H-spec with cleavage buffer. To switch buffers, we
511 dialyzed the protein against 25 mM HEPES pH 7.4, 150 mM NaCl, 1 mM TCP overnight. Then
512 the purified protein was concentrated by ultrafiltration to 30 µM and stored at -80ºC until used in
513 experiments.

514 G-actin was prepared from rabbit muscle acetone powder as reported (Lehrer and Kerwar,
515 1972) and further purified with size exclusion chromatography on a Superdex 75 pg column
516 (Cytiva, # 28989333) in buffer containing 5 mM Tris/HCl pH=8, 0.2 mM $CaCl_2$, 0.5 mM ATP, 1
517 mM DTT. G-actin was polymerized to F-actin by the addition of 10X polymerization buffer (100
518 mM HEPES pH 7.0, 500 mM KCl, 20 mM $MgCl_2$, 10 mM EDTA). *Drosophila* nonmuscle
519 myosin-2 subfragment-1-like protein (*Zip*, amino acids 1-813) was recombinantly overproduced
520 together with the myosin regulatory (*Sqh*) and essential light chain (*Mlc-c*) in the baculovirus/*Sf*9
521 insect cell system (Thermo Fisher Scientific) and prepared as described (Heissler et al., 2015).
522

523 **Co-sedimentation assays**

524 For co-sedimentation assays, β_H-Spec CH domains or myosin were incubated with F-actin
525 for 15 mins at room temperature in an assay buffer containing 10 mM HEPES pH 7.4, 100 mM
526 NaCl, 0.1 mM EGTA, 20µM ATP and 1 mM DTT and subsequently sedimented (100,000 x g, 15
527 min, 4°C, TLA-100 rotor) in an Ultima MAX-XP ultracentrifuge (Beckman). For competition

528 assays, β_H-Spec and actin were preincubated for 15 mins at room temperature before the addition
529 of myosin. Supernatant and pellet fractions were separated and the pellet fraction was resuspended
530 in an equal volume of assay buffer. Samples were supplemented with NuPAGE LDS sample buffer
531 (Invitrogen, #NP0007) and heated for 10 min at 90°C. Supernatant and pellet fractions were
532 resolved on 4-12% NuPAGE Bis-Tris polyacrylamide gels (Invitrogen, NP0323BOX). Gels were
533 incubated with PageBlue protein staining solution (Thermo Scientific, #24620) and destained with
534 water. Gels were documented with a ChemiDoc MP (Bio-Rad) and densitometric analysis was
535 performed with Fiji (Schindelin et al., 2012). Data plots and secondary analysis were performed
536 in Origin 2019.
537
538 **Model building**
539 A homology model of the *Drosophila* myosin motor domain (*Zip*, amino acids 1-813) in
540 the actin-bound state was modeled using the cryo-EM structure of the human nonmuscle myosin-
541 2C motor domain in the rigor state (PDB entry: 5JLH) as a template. Both motor domains share ~
542 72% sequence identity at the amino acid level. The motor domain model was built using Modeler
543 (Sali and Blundell, 1993). The model of the *Drosophila* β_H-spectrin calponin homology domain
544 tandem (CH1-CH2, amino acids 1-278) was modeled using ColabFold (Mirdita et al., 2022). This
545 model was superimposed onto the cryo-EM structure of the human β-III spectrin CH1 domain
546 bound to F-actin (PDB entry: 6ANU) for binding site analysis.
547
548 **ACKNOWLEDGEMENTS**

549 We thank Christian Klämbt for the β-spec antibody, and Richard Ebright and Bryce Nickels for
550 sharing equipment for protein purification. This research was supported by National Institutes of
551 Health grants R01GM143539 (KC) and GM131748 (KDI).

552

553 **DATA AVAILABILITY**

554 All data generated or analyzed during this study are included in the manuscript and supporting
555 files. Plasmids and transgenic fly lines generated in this study are all available on request

556
557 **REFERENCES**
558

559 Alegot, H., Markosian, C., Rauskolb, C., Yang, J., Kirichenko, E., Wang, Y.C., and Irvine, K.D.
560 (2019). Recruitment of Jub by alpha-catenin promotes Yki activity and Drosophila wing growth.
561 J Cell Sci *132*. 10.1242/jcs.222018.

562 Aragona, M., Panciera, T., Manfrin, A., Giulitti, S., Michielin, F., Elvassore, N., Dupont, S., and
563 Piccolo, S. (2013). A mechanical checkpoint controls multicellular growth through YAP/TAZ
564 regulation by actin-processing factors. Cell *154*, 1047-1059. 10.1016/j.cell.2013.07.042.

565 Avery, A.W., Crain, J., Thomas, D.D., and Hays, T.S. (2016). A human beta-III-spectrin
566 spinocerebellar ataxia type 5 mutation causes high-affinity F-actin binding. Sci Rep *6*, 21375.
567 10.1038/srep21375.

568 Avery, A.W., Fealey, M.E., Wang, F., Orlova, A., Thompson, A.R., Thomas, D.D., Hays, T.S.,
569 and Egelman, E.H. (2017). Structural basis for high-affinity actin binding revealed by a beta-III-
570 spectrin SCA5 missense mutation. Nat Commun *8*, 1350. 10.1038/s41467-017-01367-w.

571 Das Thakur, M., Feng, Y., Jagannathan, R., Seppa, M.J., Skeath, J.B., and Longmore, G.D.
572 (2010). Ajuba LIM proteins are negative regulators of the Hippo signaling pathway. Curr Biol
573 *20*, 657-662. 10.1016/j.cub.2010.02.035.

574 Deng, H., Wang, W., Yu, J., Zheng, Y., Qing, Y., and Pan, D. (2015). Spectrin regulates Hippo
575 signaling by modulating cortical actomyosin activity. Elife *4*, e06567. 10.7554/eLife.06567.

576 Deng, H., Yang, L., Wen, P., Lei, H., Blount, P., and Pan, D. (2020). Spectrin couples cell shape,
577 cortical tension, and Hippo signaling in retinal epithelial morphogenesis. J Cell Biol *219*.
578 10.1083/jcb.201907018.

579 Duan, R., Kim, J.H., Shilagardi, K., Schiffhauer, E.S., Lee, D.M., Son, S., Li, S., Thomas, C.,
580 Luo, T., Fletcher, D.A., et al. (2018). Spectrin is a mechanoresponsive protein shaping fusogenic

581 synapse architecture during myoblast fusion. Nat Cell Biol *20*, 688-698. 10.1038/s41556-018-
582 0106-3.

583 Dubreuil, R., Byers, T.J., Branton, D., Goldstein, L.S., and Kiehart, D.P. (1987). Drosophilia
584 spectrin. I. Characterization of the purified protein. J Cell Biol *105*, 2095-2102.
585 10.1083/jcb.105.5.2095.

586 Dubreuil, R.R., Maddux, P.B., Grushko, T.A., and MacVicar, G.R. (1997). Segregation of two
587 spectrin isoforms: polarized membrane-binding sites direct polarized membrane skeleton
588 assembly. Mol Biol Cell *8*, 1933-1942. 10.1091/mbc.8.10.1933.

589 Dye, N.A., Popovic, M., Spannl, S., Etournay, R., Kainmuller, D., Ghosh, S., Myers, E.W.,
590 Julicher, F., and Eaton, S. (2017). Cell dynamics underlying oriented growth of the Drosophila
591 wing imaginal disc. Development *144*, 4406-4421. 10.1242/dev.155069.

592 Fernandez, B.G., Gaspar, P., Bras-Pereira, C., Jezowska, B., Rebelo, S.R., and Janody, F. (2011).
593 Actin-Capping Protein and the Hippo pathway regulate F-actin and tissue growth in Drosophila.
594 Development *138*, 2337-2346. 10.1242/dev.063545.

595 Fernandez-Gonzalez, R., Simoes, S.d.M., Röper, J.-C., Eaton, S., and Zallen, J.A. (2009).
596 Myosin II dynamics are regulated by tension in intercalating cells. Developmental Cell *17*, 736-
597 743. 10.1016/j.devcel.2009.09.003.

598 Fletcher, G.C., Elbediwy, A., Khanal, I., Ribeiro, P.S., Tapon, N., and Thompson, B.J. (2015).
599 The Spectrin cytoskeleton regulates the Hippo signalling pathway. EMBO J *34*, 940-954.
600 10.15252/embj.201489642.

601 Forest, E., Logeay, R., Geminard, C., Kantar, D., Frayssinoux, F., Heron-Milhavet, L., and
602 Djiane, A. (2018). The apical scaffold big bang binds to spectrins and regulates the growth of
603 Drosophila melanogaster wing discs. J Cell Biol *217*, 1047-1062. 10.1083/jcb.201705107.

604 Greenberg, M.J., Arpag, G., Tuzel, E., and Ostap, E.M. (2016). A Perspective on the Role of
605 Myosins as Mechanosensors. Biophys J *110*, 2568-2576. 10.1016/j.bpj.2016.05.021.

606 Hamaratoglu, F., Willecke, M., Kango-Singh, M., Nolo, R., Hyun, E., Tao, C., Jafar-Nejad, H.,
607 and Halder, G. (2006). The tumour-suppressor genes NF2/Merlin and Expanded act through
608 Hippo signalling to regulate cell proliferation and apoptosis. Nat Cell Biol *8*, 27-36.
609 10.1038/ncb1339.

610 Heemskerk, I., and Streichan, S.J. (2015). Tissue cartography: compressing bio-image data by
611 dimensional reduction. Nat Methods *12*, 1139-1142. 10.1038/nmeth.3648.

612 Heissler, S.M., Chinthalapudi, K., and Sellers, J.R. (2015). Kinetic characterization of the sole
613 nonmuscle myosin-2 from the model organism Drosophila melanogaster. FASEB J *29*, 1456-
614 1466. 10.1096/fj.14-266742.

615 Heissler, S.M., and Manstein, D.J. (2013). Nonmuscle myosin-2: mix and match. Cell Mol Life
616 Sci *70*, 1-21. 10.1007/s00018-012-1002-9.

617 Hulsmeier, J., Pielage, J., Rickert, C., Technau, G.M., Klambt, C., and Stork, T. (2007). Distinct
618 functions of alpha-Spectrin and beta-Spectrin during axonal pathfinding. Development *134*, 713-
619 722. 10.1242/dev.02758.

620 Ibar, C., Kirichenko, E., Keepers, B., Enners, E., Fleisch, K., and Irvine, K.D. (2018). Tension-
621 dependent regulation of mammalian Hippo signaling through LIMD1. J Cell Science *131*,
622 jcs214700.

623 Jia, Y., Shen, D., Wang, X., Sun, J., Peng, P., Xu, R.G., Xu, B., and Ni, J.Q. (2019). flySAM
624 Transgenic CRISPRa System Manual. Bio Protoc *9*, e3147. 10.21769/BioProtoc.3147.

625 Jia, Y., Xu, R.G., Ren, X., Ewen-Campen, B., Rajakumar, R., Zirin, J., Yang-Zhou, D., Zhu, R.,
626 Wang, F., Mao, D., et al. (2018). Next-generation CRISPR/Cas9 transcriptional activation in
627 Drosophila using flySAM. Proc Natl Acad Sci U S A *115*, 4719-4724.
628 10.1073/pnas.1800677115.

629 Khanna, M.R., Mattie, F.J., Browder, K.C., Radyk, M.D., Crilly, S.E., Bakerink, K.J., Harper,
630 S.L., Speicher, D.W., and Thomas, G.H. (2015). Spectrin tetramer formation is not required for
631 viable development in Drosophila. J Biol Chem *290*, 706-715. 10.1074/jbc.M114.615427.

632 Kiehart, D.P., and Feghali, R. (1986). Cytoplasmic myosin from Drosophila melanogaster. J Cell
633 Biol *103*, 1517-1525. 10.1083/jcb.103.4.1517.

634 Krueger, D., Pallares Cartes, C., Makaske, T., and De Renzis, S. (2020). betaH-spectrin is
635 required for ratcheting apical pulsatile constrictions during tissue invagination. EMBO Rep *21*,
636 e49858. 10.15252/embr.201949858.

637 Lee, J.K., Brandin, E., Branton, D., and Goldstein, L.S. (1997). alpha-Spectrin is required for
638 ovarian follicle monolayer integrity in Drosophila melanogaster. Development *124*, 353-362.

639 Lehrer, S.S., and Kerwar, G. (1972). Intrinsic fluorescence of actin. Biochemistry *11*, 1211-1217.
640 10.1021/bi00757a015.

641 Liem, R.K. (2016). Cytoskeletal Integrators: The Spectrin Superfamily. Cold Spring Harb
642 Perspect Biol *8*. 10.1101/cshperspect.a018259.

643 Lye, C.M., Naylor, H.W., and Sanson, B. (2014). Subcellular localisations of the CPTI collection
644 of YFP-tagged proteins in Drosophila embryos. Development *141*, 4006-4017.
645 10.1242/dev.111310.

646 Machnicka, B., Czogalla, A., Hryniewicz-Jankowska, A., Boguslawska, D.M., Grochowalska,
647 R., Heger, E., and Sikorski, A.F. (2014). Spectrins: a structural platform for stabilization and
648 activation of membrane channels, receptors and transporters. Biochim Biophys Acta *1838*, 620-
649 634. 10.1016/j.bbamem.2013.05.002.

650 Martin, A.C., Kaschube, M., and Wieschaus, E.F. (2009). Pulsed contractions of an actin-myosin
651 network drive apical constriction. Nature *457*, 495-499. 10.1038/nature07522.

652 Mirdita, M., Schutze, K., Moriwaki, Y., Heo, L., Ovchinnikov, S., and Steinegger, M. (2022).
653 ColabFold: making protein folding accessible to all. Nat Methods *19*, 679-682. 10.1038/s41592-
654 022-01488-1.

655 Misra, J.R., and Irvine, K.D. (2018). The Hippo Signaling Network and its Biological Functions.
656 Annual Reviews of Genetics *52*, 3.1-3.23.

657 Nagarkar-Jaiswal, S., Lee, P.T., Campbell, M.E., Chen, K., Anguiano-Zarate, S., Gutierrez,
658 M.C., Busby, T., Lin, W.W., He, Y., Schulze, K.L., et al. (2015). A library of MiMICs allows
659 tagging of genes and reversible, spatial and temporal knockdown of proteins in Drosophila. Elife
660 *4*. 10.7554/eLife.05338.

661 Noll, N., Mani, M., Heemskerk, I., Streichan, S.J., and Shraiman, B.I. (2017). Active tension
662 network model suggests an exotic mechanical state realized in epithelial tissues. Nature Physics
663 *13*, 1221-1226.

664 Pan, Y., Alegot, H., Rauskolb, C., and Irvine, K.D. (2018). The dynamics of Hippo signaling
665 during Drosophila wing development. Development *145*. 10.1242/dev.165712.

666 Pan, Y., Heemskerk, I., Ibar, C., Shraiman, B.I., and Irvine, K.D. (2016). Differential growth
667 triggers mechanical feedback that elevates Hippo signaling. Proc Natl Acad Sci U S A *113*,
668 E6974-E6983. 10.1073/pnas.1615012113.

669 Papal, S., Cortese, M., Legendre, K., Sorusch, N., Dragavon, J., Sahly, I., Shorte, S., Wolfrum,
670 U., Petit, C., and El-Amraoui, A. (2013). The giant spectrin betaV couples the molecular motors
671 to phototransduction and Usher syndrome type I proteins along their trafficking route. Hum Mol
672 Genet *22*, 3773-3788. 10.1093/hmg/ddt228.

673 Pogodalla, N., Kranenburg, H., Rey, S., Rodrigues, S., Cardona, A., and Klambt, C. (2021).
674 Drosophila ssHeavy-Spectrin is required in polarized ensheathing glia that form a diffusion-
675 barrier around the neuropil. Nat Commun *12*, 6357. 10.1038/s41467-021-26462-x.

676 Rauskolb, C., Cervantes, E., Madere, F., and Irvine, K.D. (2019). Organization and function of
677 tension-dependent complexes at adherens junctions. J Cell Sci *132*. 10.1242/jcs.224063.

678 Rauskolb, C., Han, A., Kirichenko, E., Ibar, C., and Irvine, K.D. (2022). Analysis of the
679 Drosophila Ajuba LIM protein defines functions for distinct LIM domains. PLoS One *17*,
680 e0269208. 10.1371/journal.pone.0269208.

681 Rauskolb, C., Pan, G., Reddy, B.V., Oh, H., and Irvine, K.D. (2011). Zyxin links fat signaling to
682 the hippo pathway. PLoS Biol *9*, e1000624. 10.1371/journal.pbio.1000624.

683 Rauskolb, C., Sun, S., Sun, G., Pan, Y., and Irvine, K.D. (2014). Cytoskeletal tension inhibits
684 Hippo signaling through an Ajuba-Warts complex. Cell *158*, 143-156.
685 10.1016/j.cell.2014.05.035.

686 Razzell, W., Bustillo, M.E., and Zallen, J.A. (2018). The force-sensitive protein Ajuba regulates
687 cell adhesion during epithelial morphogenesis. J Cell Biol, jcb.201801171.

688 Royou, A., Field, C., Sisson, J.C., Sullivan, W., and Karess, R. (2004). Reassessing the role and
689 dynamics of nonmuscle myosin II during furrow formation in early Drosophila embryos. Mol
690 Biol Cell *15*, 838-850. 10.1091/mbc.e03-06-0440.

691 Sabino, D., Brown, N.H., and Basto, R. (2011). Drosophila Ajuba is not an Aurora-A activator
692 but is required to maintain Aurora-A at the centrosome. J Cell Sci *124*, 1156-1166.
693 10.1242/jcs.076711.

694 Sali, A., and Blundell, T.L. (1993). Comparative protein modelling by satisfaction of spatial
695 restraints. J Mol Biol *234*, 779-815. 10.1006/jmbi.1993.1626.

696 Sansores-Garcia, L., Bossuyt, W., Wada, K., Yonemura, S., Tao, C., Sasaki, H., and Halder, G.
697 (2011). Modulating F-actin organization induces organ growth by affecting the Hippo pathway.
698 EMBO J *30*, 2325-2335. 10.1038/emboj.2011.157.

699 Sarpal, R., Yan, V., Kazakova, L., Sheppard, L., Yu, J.C., Fernandez-Gonzalez, R., and Tepass,
700 U. (2019). Role of α-Catenin and its mechanosensing properties in regulating Hippo/YAP-
701 dependent tissue growth. PLoS Genet *15*, e1008454. 10.1371/journal.pgen.1008454.

702 Schindelin, J., Arganda-Carreras, I., Frise, E., Kaynig, V., Longair, M., Pietzsch, T., Preibisch,
703 S., Rueden, C., Saalfeld, S., Schmid, B., et al. (2012). Fiji: an open-source platform for
704 biological-image analysis. Nat Methods *9*, 676-682. 10.1038/nmeth.2019.

705 Sellers, J.R., Eisenberg, E., and Adelstein, R.S. (1982). The binding of smooth muscle heavy
706 meromyosin to actin in the presence of ATP. Effect of phosphorylation. J Biol Chem *257*,
707 13880-13883.

708 Sun, S., Reddy, B.V., and Irvine, K.D. (2015). Localization of Hippo signalling complexes and
709 Warts activation in vivo. Nat Commun *6*, 8402. 10.1038/ncomms9402.

710 Thomas, G.H., and Kiehart, D.P. (1994). Beta heavy-spectrin has a restricted tissue and
711 subcellular distribution during Drosophila embryogenesis. Development *120*, 2039-2050.
712 10.1242/dev.120.7.2039.

713 Thomas, G.H., Zarnescu, D.C., Juedes, A.E., Bales, M.A., Londergan, A., Korte, C.C., and
714 Kiehart, D.P. (1998). Drosophila betaHeavy-spectrin is essential for development and contributes
715 to specific cell fates in the eye. Development *125*, 2125-2134. 10.1242/dev.125.11.2125.

716 Vasquez, C.G., Heissler, S.M., Billington, N., Sellers, J.R., and Martin, A.C. (2016). Drosophila
717 non-muscle myosin II motor activity determines the rate of tissue folding. Elife *5*.
718 10.7554/eLife.20828.

719 von der Ecken, J., Heissler, S.M., Pathan-Chhatbar, S., Manstein, D.J., and Raunser, S. (2016).
720 Cryo-EM structure of a human cytoplasmic actomyosin complex at near-atomic resolution.
721 Nature *534*, 724-728. 10.1038/nature18295.

722 Winter, C.G., Wang, B., Ballew, A., Royou, A., Karess, R., Axelrod, J.D., and Luo, L. (2001).
723 Drosophila Rho-associated kinase (Drok) links Frizzled-mediated planar cell polarity signaling
724 to the actin cytoskeleton. Cell *105*, 81-91.

725 Wong, K.K., Li, W., An, Y., Duan, Y., Li, Z., Kang, Y., and Yan, Y. (2015). beta-Spectrin
726 regulates the hippo signaling pathway and modulates the basal actin network. J Biol Chem *290*,
727 6397-6407. 10.1074/jbc.M114.629493.

728 Xie, S., and Martin, A.C. (2015). Intracellular signalling and intercellular coupling coordinate
729 heterogeneous contractile events to facilitate tissue folding. Nat Commun *6*, 7161.
730 10.1038/ncomms8161.

731 Zarnescu, D.C., and Thomas, G.H. (1999). Apical spectrin is essential for epithelial
732 morphogenesis but not apicobasal polarity in Drosophila. J Cell Biol *146*, 1075-1086.
733 10.1083/jcb.146.5.1075.

734 Zheng, Y., and Pan, D. (2019). The Hippo Signaling Pathway in Development and Disease. Dev
735 Cell *50*, 264-282. 10.1016/j.devcel.2019.06.003.
736